2D materials for tunable and nonlinear metaoptics

Zeng Wang[#], Kandammathe Valiyaveedu Sreekanth[#], Meng Zhao[#], Jinpeng Nong, Yincheng Liu, Jinghua Teng*

Institute of Materials Research and Engineering (IMRE), Agency for Science, Technology and Research (A*STAR), 2 Fusionopolis Way, Innovis #08-03, Singapore 138634, Republic of Singapore

[#]These authors contribute equally to the work

*Corresponding author: Jinghua Teng (jh-teng@imre.a-star.edu.sg)

Abstract

Metaoptics formed by ultrathin and planar building blocks enable compact and efficient optical devices that manipulate light at the nanoscale. The development of tunable metaoptics holds the promise of miniaturized and efficient optical systems that can dynamically adapt to changing conditions or requirements, propelling innovations in fields ranging from telecommunication and imaging to quantum computing and sensing. Two-dimensional (2D) materials show strong promises in enabling tunable metaoptics due to their exceptional electronic and optical properties from the quantum confinement within the atomically thin layers. In this review, we discuss the recent advancements and challenges of 2D material-based tunable metaoptics in both linear and nonlinear regimes and provide an outlook for prospects in this rapidly advancing area.

Introduction

The advent of flat optics or metaoptics heralds a significant transformation in optical technology, blending with the pursuit of replacing traditional bulky optical components with planar and compact alternatives. [1–4] It is bringing revolution to not only the optics design and functionality, but also the ways of manufacturing optics and related optical systems for applications [5–10] like optical communication, imaging, and sensing. Despite rapid progress in metaoptics, the insignificant changes in the complex permittivity in their building blocks made of metals, dielectrics, or bulk semiconductors under external influences limit the approaches to tune their

plasmonic or Mie resonance, thus undermine their potentials for dynamic light control that could bring forth many new phenomena and applications. Various tunable and reconfigurable metaoptics based on different materials and mechanisms have been investigated [5,11,12], including liquid crystals [13–15] and phase change materials[16–19] that demonstrated relatively large refractive index tuning under electrical control. 2D materials show extraordinary potential from their exceptional electronic and optical characteristics shaped by quantum confinement within a few atoms thickness, which lead to distinctive excitonic effects not found in bulk materials [20–22].

The tunability of excitonic resonance in 2D materials has emerged as a possible avenue for the next generation of ultrathin metaoptics [23–26]. For example, the reduced dielectric screening in atomically thin transition metal dichalcogenides (TMDCs) enhances exciton binding energies, surpassing the room temperature (RT) thermal energy of about 0.026 eV. This results in robust excitons in TMDCs and creates a versatile platform for manipulating exciton resonance through strong light-matter interaction to enable dynamics and wide-range complex refractive index control [27,28]. In addition to neutral excitons, recent research has uncovered a variety of closely associated quasiparticles, like charged excitons or trions, which also play a significant role in 2D systems [29–34]. These quasiparticles notably impact the system's tunability up to room temperature, a phenomenon uncommon in bulk semiconductors. The coexistence of excitons and trions is particularly influential for 2D tunable metaoptics, as it directly alters the optical properties of these systems. Consequently, a thorough understanding of trionic behaviour is essential for achieving optimal performance in such devices.

In the near field, the highly tunable polaritons in 2D materials offer a concrete avenue to surpass the diffraction limit and achieve light manipulation in extremely confined space. Polaritons are a class of quasiparticles that originate from the coupling between photons and collective excitations. For example, plasmon polaritons are formed when the collective oscillation of electrons in metals, i.e., plasmons, is coupled with photons, while phonon polaritons are formed when collective lattice vibrations, i.e., phonons, are coupled with photons. 2D polaritons are believed to hold tremendous potential in advancing nanophotonics because of their high susceptibility to external stimuli. Surface plasmon polaritons in graphene have been extensively studied for their strong light field confinement and good tunability in the mid-far infrared range [35,36], and phonon polaritons with hyperbolic dispersion in structured graphene, hexagonal boron nitride (h-BN), and other 2D

materials have been used to demonstrated hyperbolic metasurfaces [37–39]. What makes 2D polaritons even more intriguing is that the topological and quantum states in 2D materials open new opportunities to understand, engineer and utilize polaritons in 2D materials.

Besides the linear regime, metaoptics have recently emerged as a promising platform to study the nonlinear optical phenomena bearing the merits of loosened phase matching requirements in sub-wavelength dimension, strongly enhanced light-matter interaction due to field confinement or high Q resonance, and the much smaller light interaction scale than the light coherence length [40–45]. The large nonlinear optical coefficients discovered in 2D materials, besides the tunable exciton and polariton resonance, the broadband optical response and strong interlayer coupling, make 2D materials natural candidates for nonlinear optics [46–50]. Integrating metaoptics with two-dimensional materials holds immense potential for significantly enhancing and even tuning nonlinear effects, paving the way for the discovery of novel phenomena and more efficient applications.

This review explores the cutting-edge developments in the unique excitonic and polaritonic effects in 2D materials and their significant impact on metaoptics. It delves into the basic physics underlying excitons and quasiparticles in 2D materials, highlights the progress in metaoptics driven by the tunability of excitonic resonance, especially for TMDCs working in the visible range, and examines the creative methods employed to incorporate 2D materials into adaptable optical applications. It further discusses in particular tunable polaritons in manipulating and enhancing light-matter interactions in highly confined space in materials like graphene and TMDCs. It also highlights the nonlinear optical properties of these materials, accentuating their potential in creating ultra-compact and energy-efficient optoelectronic components. The synergy of these nonlinear phenomena with the versatile electronic and mechanical properties of 2D materials, particularly when integrated into heterostructures, opens new avenues for the development of advanced photonic and optoelectronic systems with customizable and dynamic functionalities. By examining both the current challenges and future research arenas, this review seeks to offer insights into the utilization of 2D materials for creating a novel category of tunable metaoptics, with the potential of transforming the field of optical technologies.

2D excitons for tunable metaoptics

Fundamentals of Excitons in 2D Materials

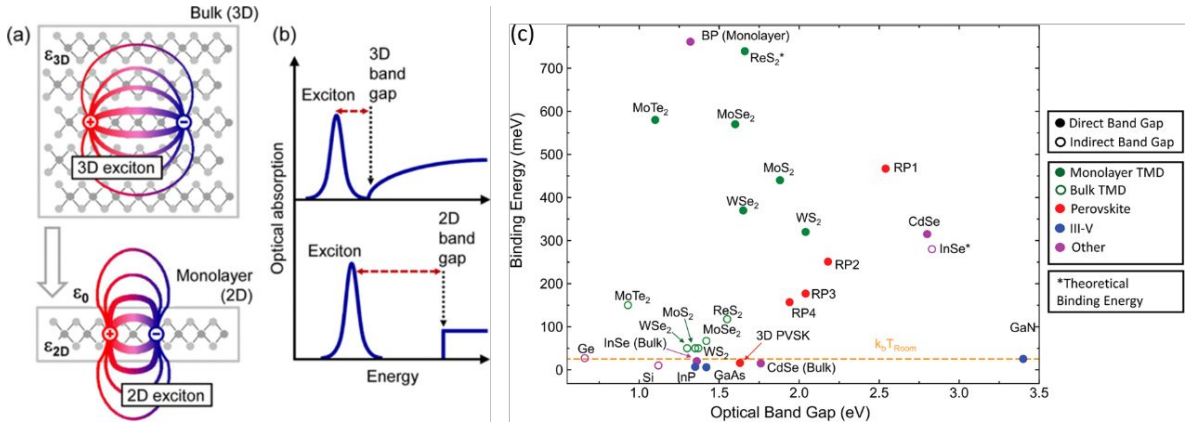

Figure 1. (a) electrons and holes bound into excitons for the three-dimensional (3D) bulk and 2D materials. **(b)** The transition from 3D to 2D is expected to lead to an increase of both the band gap and the exciton binding energy (indicated by the dashed red line) **(c)** Binding energy of excitons in some common 3D and 2D semiconductors. The yellow dotted line represents the thermal energy at room temperature. Figure 1(a) and (b) reproduced with permission from [51] © 2014-APS, Figure 1(c) reproduced with permission from [52] © 2022-AIP

Excitons are quasiparticles consisting of an electron and a hole bound together by their electrostatic Coulomb attraction. They play a crucial role in the optical and electronic properties of 2D materials, particularly in TMDCs. Due to strong spatial confinement and reduced dielectric screening, their binding energies are significantly higher than those in bulk materials [51]. In 3D semiconductors, the exciton binding energy (E_b) could be estimated by using the hydrogen model as below when neglecting the quantum defect:

$$E_b^{3D}(n) = \frac{R_Y}{n^2}$$

Here R_Y is Rydberg constant for excitons, and n is quantum number. While in two dimensions, due to the quantum confinement influencing the exciton radius and average dielectric constant, the Rydberg exciton binding energy is modified as:

$$E_b^{2D}(n) = \frac{R_Y}{\left(n - \frac{1}{2}\right)^2}$$

This implies that the lowest 2D exciton binding energy (n=1) has a magnitude four times larger than the 3D one at ground state, as demonstrated in Figure 1(a) and 1(b). Experimentally, binding energies of excitons can range from a few hundred meV to over 1 eV in 2D materials as shown in Figure 1(c). For example, the A exciton in monolayer MoS_2 has a binding energy of approximately 0.5 eV, which is substantially greater than the thermal energy at RT (26 meV) and the binding energies of typical bulk semiconductors like GaAs (~ 15 meV). Therefore, excitons are highly stable in monolayer TMDCs even at RT. It is important to note that the reported binding energy values for the same material can differ significantly across various studies due to differences in material quality, the dielectric environment, experimental conditions, and other factors.

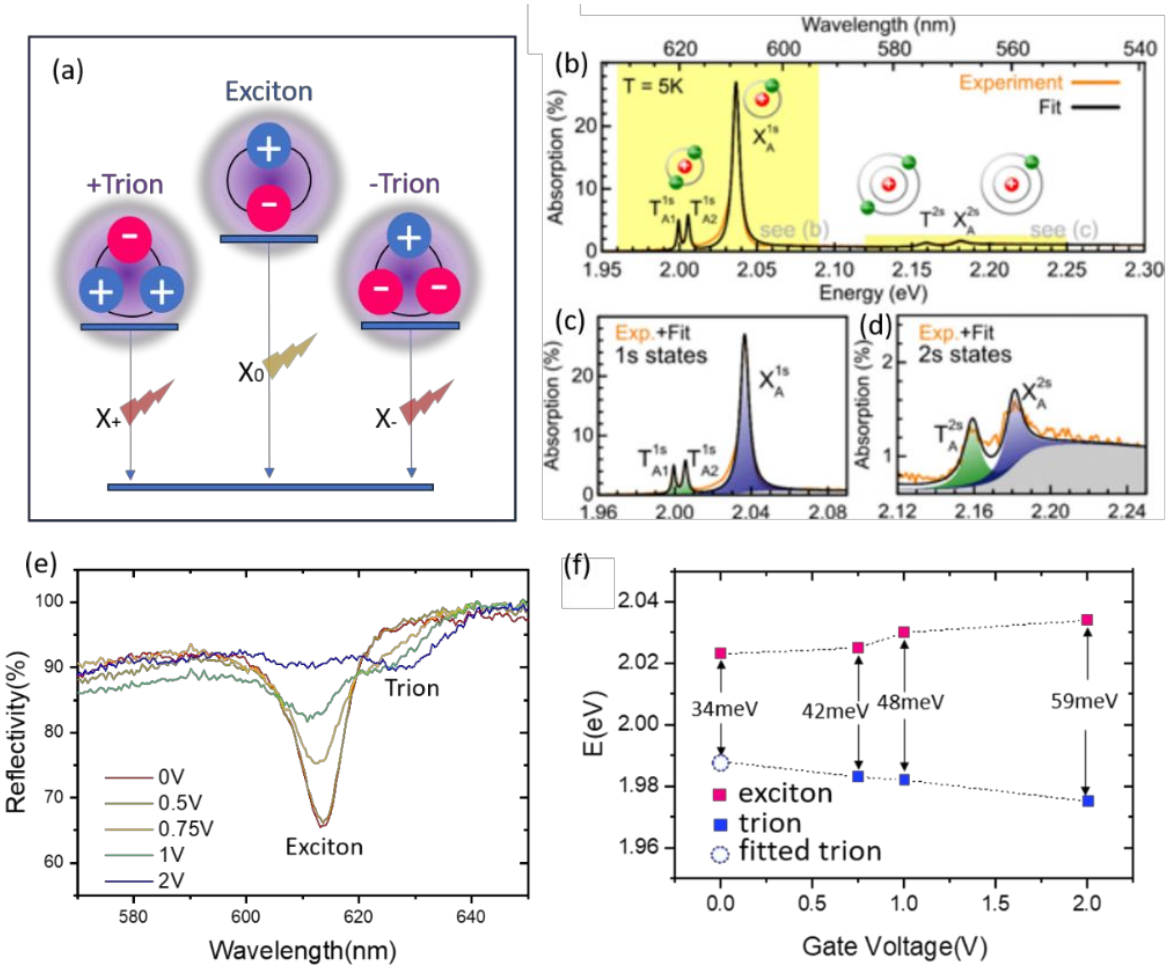

Figure 2. (a) Illustration of the exciton and trion. **(b)** Optical absorption spectrum of a h-BN-encapsulated WS_2 monolayer measured at T=5 K. **(c)** Experimental and fitted spectra for (n=1) states, where shaded green and blue regions represent the contributions from trions and excitons, respectively. **(d)** Zoomed-in view highlighting (n=2) excited state trions and excitons. **(e)** Cavity enhanced exciton-trion resonance at RT. **(f)** WS_2 trion binding energy measured at RT. Figure. 2(a) – (d) reproduced with permission from [53] © 2019 – APS, Figure. 2(e) – (f) reproduced with permission from [54] © 2023 – Wiley

Besides neutral excitons, trions in 2D TMDCs are more complex quasiparticles involving two electrons and one hole or two holes and one electron bound together, forming negatively or positively charged excitons, respectively, as illustrated in Figure 2(a). The presence of trions significantly influences the optical properties of TMDCs. When discussing trions, it is also essential to consider their binding energy, which is typically much lower than that of neutral excitons due to the additional electron or hole [34,51,52]. The binding energy of trions can be estimated by considering the additional electron-hole Coulomb interaction and is expressed as: $E_{binding\ trion} = E_{exciton} - E_{trion}$. It is indeed worth noting that the observation of trion binding energy is very limited due to the difficulties in obtaining accurate and reliable measurements of reflectance in ultrathin samples under doping from the weak light-matter interaction. Among various reports [55–57], a direct absorption measurement estimated WS_2 trion binding energy around 31 meV to 37 meV at 5 K based on h-BN encapsulated samples, as shown in Figure 2(b) – 2(d) [53], and another study using reflectance contrast spectra reported the zero-density trion binding energy of 23 meV at 50 K [58]. Thanks to the cavity effect, Z. Wang *et al*. has recently determined the trion binding energy via the reflectance at RT to be around 42 meV in slightly n-doped condition and estimated to be around 34 meV in the zero-density at zero bias by extrapolating the linearly fitted trion binding energies under different voltages, as shown in Figure 2(e) and 2(f) [54].

The impact of trions on tunable metaoptics is profound. The tunability comes from the ability to control the charge carrier concentration in TMDCs through gating, doping, or photoexcitation, which directly affects the trion population and, consequently, the optical response of the material. For instance, by applying an electrical field through a gate, one can modulate the free carrier concentration, thus switching between exciton and trion resonances. This effect can be used to dynamically control the reflectance, transmittance, and absorption of light in metaoptics, making trions an active element for reconfigurable photonics.

Excitonic Tunability in 2D Materials for Active Metaoptics

Although the excitonic resonance has strong oscillation strength, the very limited interaction length still results in an insignificant overall optical response. To enhance excitonic resonances, the encapsulation of TMDCs with h-BN under low-temperature working conditions has been adapted for various 2D devices. h-BN encapsulation provides a cleaner, more stable, and protective environment for TMDCs, leading to enhanced excitonic and trionic properties, while operation at low temperatures mitigates phonon scattering and thermal broadening, resulting in sharper excitonic resonances.

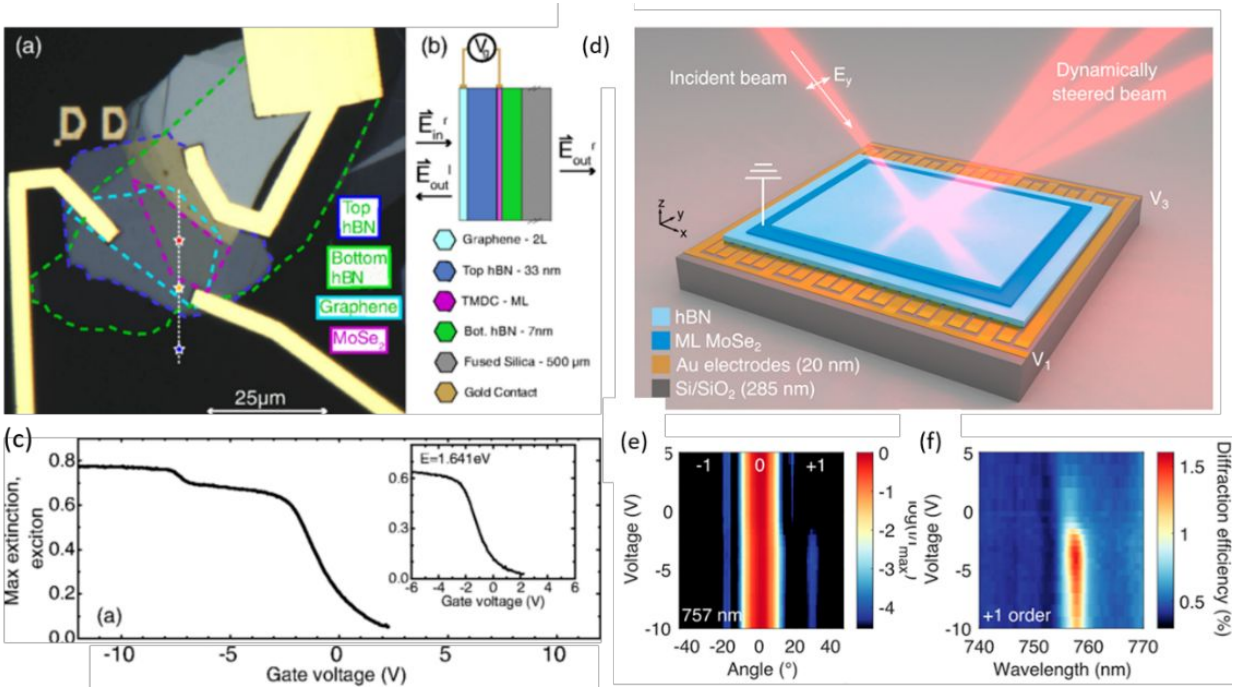

Figure 3. The excitonic metaoptics working at low temperature. (a) Micrograph of the measured heterostructure. The $MoSe_2$ monolayer is encapsulated between 33 nm (top) and 7 nm (bottom) thick h-BN layers. **(b)** Interaction of an incident field with a $MoSe_2$ monolayer. **(c)** Gate voltage (V_g) dependence of the maximal extinction of transmitted light using the exciton resonance. **(d)** Schematic of the exciton-based TMDC metaoptics for dynamic beam steering. **(e)** Beam steering angle under the applied asymmetric voltage gradient. **(f)** Voltage and spectral dependence of the diffraction efficiency. Figure 3(a) – (c) reproduced with permission from [59] © 2018 - APS, Figure 3(d) – (f) reproduced with permission from [60] © 2023 - ACS

In the studies by P. Back *et al.*, a single $MoSe_2$ monolayer was used to create an electrically tunable mirror [59]. As shown in Figure 3(a)-3(c), $MoSe_2$ is sandwiched between two layers of h-BN which

acted as a resonant cavity, enhancing light interaction with the excitonic resonance. At around 4 K, exciton decay became purely radiative and the encapsulated $MoSe_2$ flakes showed strong tunable exciton resonance, producing adjustable transmission from 10% to 60%. Y. Zhou *et al.* also reported similar results [61]. Very recently, M. Li *et al.* advanced the function of h-BN encapsulated $MoSe_2$ for dynamically steering beams between -30° and 30° via varying gate voltage, displayed in Figure 3(d)-3(f) [60]. Although the demonstrations were on small $MoSe_2$ flakes at cryogenic temperatures, these initial examples have shown that single-layer TMDCs can attain significant optical efficiencies with the added advantage of electrical manipulation of their optical properties.

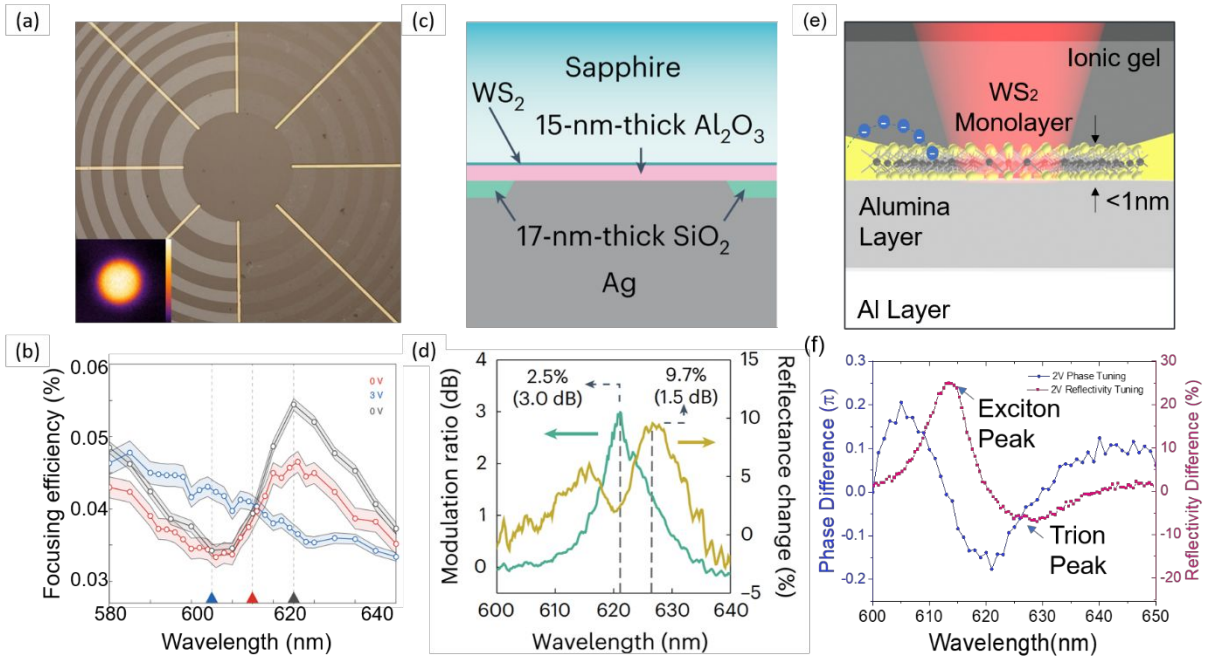

Figure 4. The excitonic metaoptics working at RT. (a) A Fresnel zone plate lens made on monolayer WS_2. **(b)** Excitonic modulation of the light intensity in the focusing spot of the WS_2 zone plate lens. **(c)** A monolayer WS_2 free-space optical modulator based on a MOS capacitor configuration. **(d)** Modulation ratio (green) and absolute reflectance change (yellow) spectra. A 3 dB modulation ratio and a 10% reflectance change are observed in the experiment. **(e)** Al/Al_2O_3 cavity effect to enhance the excitonic resonance of monolayer WS_2. **(f)** Dynamic phase and amplitude tuning with enhanced excitonic and trionic resonances in monolayer WS2. Figure 4(a) and 4(b) reproduced with permission from [62] © 2020 – Nature, Figure 4(c) and 4(d) reproduced with permission from [63] © 2023 – Nature, Figure 4(e) and 4(f) reproduced with permission from [54] © 2023 – Wiley

Towards realizing practical excitonic metaoptics, it is essential to develop the ability for devices to work at RT. WS_2 has been identified as a promising candidate to maintain the relatively strong oscillator strength of excitons at RT. As shown in Figure 4(a) and 4(b) [62], a Fresnel zone plate lens with a diameter of 1 mm is patterned from a large-area monolayer WS_2 grown on sapphire via chemical vapor deposition. This lens has been designed to operate optimally at wavelengths close to the exciton resonance and has a focal length of 2 mm. The 33% active modulation of focusing efficiency has been shown via exciton resonance tuning. Although the absolute absorption tuning is less than 1%, this first demonstration of exciton resonance tuning in large-area TMDCs sample highlights the opportunities that excitons offer for tunable metaoptics. The demonstrated enhanced tunability of exciton resonances via metasurface [63]. In Figure 4(c) and 4(d), a 10% reflectance change as well as a 3 dB signal modulation have been demonstrated by utilizing an aluminium/alumina (Al/Al_2O_3) optical cavity [54], as depicted in Figure 4(e). This approach overcomes the challenge of weak resonance and high optical losses in TMDCs at RT, specifically concerning trion states. The outcome is a notable electrical modulation in both amplitude and phase for exciton and trion states. Figure 4(f) shows absolute reflectance change of 25% for excitons and 7% for trions, with phase adjustments of 0.2π for excitons and 0.1π for trions, respectively. The findings reveal that trions play a key role in the electrical tuning of TMDCs devices even at RT.

Tunable excitonic metaoptics is an emerging field with vast potential, yet there are challenges need to be addressed to realize its full transformative power. One issue is the precise control of the external stimuli required to tune the excitonic properties as non-uniform electrostatic gating across a large area can result in uneven tuning of the optical properties. Another issue is the inherent narrowband nature of excitonic resonance that limits the operational bandwidth of metaoptics. These characteristics, while beneficial for certain applications requiring high selectivity, restrict the use of excitonic metaoptics in broadband applications. Potential strategies include the use of multiple materials with staggered resonances as well as interlayer excitons/trionic properties to create broader or multiple resonant peaks. While challenges abound, the field of tunable excitonic metaoptics is full of opportunities and will witness more advancement for next generation ultracompact tunable metaoptics in near future.

Tunable plasmon and phonon polaritons in 2D materials

Plasmon and phonon polaritons in 2D materials share the commonality of enabling confined and enhanced light-matter interactions at the nanoscale, leading to highly tunable optical properties [64]. These interactions allow for precise control over light propagation, frequency, and intensity, which is critical for tunable metaoptics [65]. By leveraging the adjustable nature of plasmon and phonon polaritons in 2D materials, metaoptics can be designed to dynamically modulate light, facilitating advanced functionalities like phase manipulation, amplitude control, and polarization conversion [66]. This paves the way for creating tunable and reconfigurable optical devices and systems capable of adapting their responses to changing external conditions, thus offering a versatile platform for innovative photonic applications in sensing, imaging, and information processing.

Tunable plasmon polaritons

Plasmon polaritons are electromagnetic wave-induced collective electron oscillations at the metal/dielectric interface that enable the manipulation of light-matter interactions beyond the diffraction limit. Over the past decades, this phenomenon has offered opportunities for technological advancements in various applications [67–69]. The recent advent of graphene, along with other emerging 2D materials, has further propelled the fields by providing a new platform for metaoptics that significantly complements traditional metals, dielectrics, and semiconductors. As an atomically thin 2D Dirac semimetal, doped graphene is recognized to support extremely confined plasmons (~10^6 smaller than the diffraction limit) in mid- and far-infrared (IR) and terahertz (THz) region, enabling the strong light-matter interactions[70]. The highly confined plasmon polaritons in graphene can be visualized by using the technique of scattering-type scanning near-field optical microscope (s-SNOM)[71,72], in which the photons scattered by an atomic force microscope (AFM) tip are used as the excitation source to overcome the momentum mismatch between free-space photon and plasmon [73]. On the other hand, plasmonic dissipation has been a major obstacle to realizing low-loss graphene plasmonic modes due to the electron-electron scattering in graphene and electron-phonon scattering at the interface between graphene and substrates. While conducting experiments at low temperature can reduce the intrinsic electron-electron scattering, encapsulating graphene with h-BN is an effective way to reduce the electron-phonon scattering. It has been shown that the propagation length of plasmon polaritons in h-BN encapsulated graphene can be significantly improved compared to the usual case in bare graphene on SiO_2 [74]. Low temperature SNOM measurement down to 60 K has revealed that the lifetime of

graphene plasmon can reach up to 1.6 ps, which is larger than the room temperature value by one order of magnitude [75].

The most exciting feature of graphene lies in its highly tunable conductivity via doping. In contrast to bulk metals where the substantial density of free electrons nearly shields external electric fields, graphene is a semimetal characterized by its limited density of states. Its 2D nature enables the efficient induction of free electrons or holes through chemical doping or electrical gating [76,77]. As a result, the optical response of devices based on graphene plasmon polaritons can be actively manipulated in a way that was not possible before [78,79]. This property of graphene plasmon polaritons makes it an ideal candidate to achieve integrated, multifunctional and compact mid-IR metaoptics, such as tunable infrared sources [80], modulators [81], sensors [82,83] and photodetectors [84,85], to mention a few. For example, Brar *et al*. demonstrated that graphene plasmonic resonators can generate blackbody radiation [80], featuring narrow spectral emission peaks in the mid-IR region (Figure 5(a)). Additionally, the frequency and intensity of these spectral responses can be actively modulated by applying external electric fields (Figure 5(b)). Due to the strongly confined mode volumes, a large Purcell factor of up to 10^7 can be achieved in graphene plasmonic resonators, enabling a much faster thermal emission modulation rate compared to other tuning mechanisms like using phase change materials. This also makes it suitable for designing spatial light modulators in min-infrared. Kim. *et al.* presented a graphene plasmonic device for the effective transmission of light modulation at 1397 cm^{-1} (7.16 μm) with 28.6% efficiency [81].

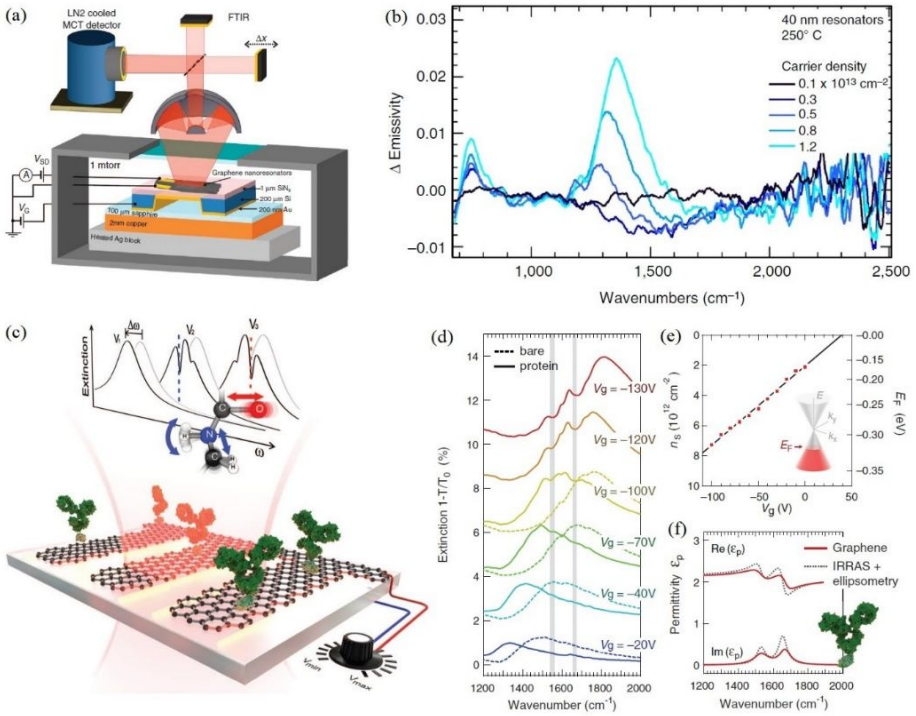

Figure 5. Tunable graphene plasmon polaritons for mid-IR applications. (a) Schematic of tunable graphene plasmonic resonator for mid-IR radiation. (**b)** Carrier density dependence of the change in emissivity. (**c)** Conceptual view of tunable graphene plasmonic biosensor. (**d)** Extinction spectra of the sensor for bias voltages from –20 V to –130 V before (dashed curves) and after (solid curves) protein bilayer formation. (**e)** Graphene carrier density (n_s) and Fermi energy (E_F) were extracted from experimental IR extinction spectra at different voltages. (**f)** The permittivity of the protein bilayer extracted from the experimental IR spectra (solid red curves) compared to the permittivity extracted from infrared reflection absorption spectroscopy (IRRAS) and ellipsometry measurements (dashed black curves). Figure 5(a) and 5(b) reproduced from [80] with CC license, Figure 5(c) - 5(f) reproduced with permission from [82] © 2015 – AAAS.

Another important application of tunable graphene plasmon polaritons is mid-IR sensing and detection. Rodrigo *et al*. demonstrated an electronically tunable graphene plasmonic biosensor for specific label-free detection of protein monolayers [82], as shown in Figure 5(c). By gate-tuning graphene Fermi levels, the resonant frequencies of the biosensor are dynamically tuned to selectively probe the protein at different frequencies, allowing the effective extraction of the refractive index of the protein (Figure 5(d)-(f)). Moreover, the highly confined graphene plasmon enables unprecedented overlap with nanoscale biomolecules, offering stronger light-protein interactions beyond state-of-the-art metallic plasmonic sensors. The ability to enhance the light

absorption in mid-infrared by graphene plasmon also makes it suitable for room temperature infrared detection based on the photo-thermoelectric effect [84,85]. With careful design of graphene plasmonic resonant structures, the graphene carrier temperature can be manipulated by the plasmonic excitation of Dirac fermions, which can be controlled by gate-tuning graphene Fermi level. Such specifically designed wavelength-tunable mid-IR photodetectors exhibit outstanding performance at room temperature, promising a very potential strategy for uncooled, tunable, and multispectral infrared detection.

While electrostatic gating is very effective in tuning graphene plasmon, the layered structure of graphene also accommodates other possibilities, such as interlayer coupling. Because of interlayer charge tunnelling, not only the plasmon wavelength is modified in bilayer graphene but also a turnoff regime for plasmon polariton in bilayer graphene appeared [86]. Furthermore, in a bilayer graphene with a controlled twist angle of 1.1º, chiral and slow plasmon polaritons have been observed [87]. Interface control of plasmon also applies to heterojunctions between graphene and other 2D materials. For example, in graphene/twisted-WSe_2 heterostructures, the ferroelectric domain of twisted-WSe_2 is imprinted onto the graphene plasmon, forming a domain-like interference pattern when imaged with s-SNOM [88]. Such a strong interfacial effect implies that graphene plasmon polaritons provide a novel approach to image the electronic structures of interacting layers, for instance, the ferroelectric domain.

Black phosphorus (BP) also supports mid-IR plasmons due to its low carrier density. In contrast to isotropic graphene, BP has a highly anisotropic crystalline structure with highly anisotropic and hyperbolic plasmons that have been theoretically studied [89]. Despite challenges such as the low air stability and difficulties in large-scale synthesis, tunable and anisotropic mid-IR plasmon has been observed in modified BP grating structures [90].

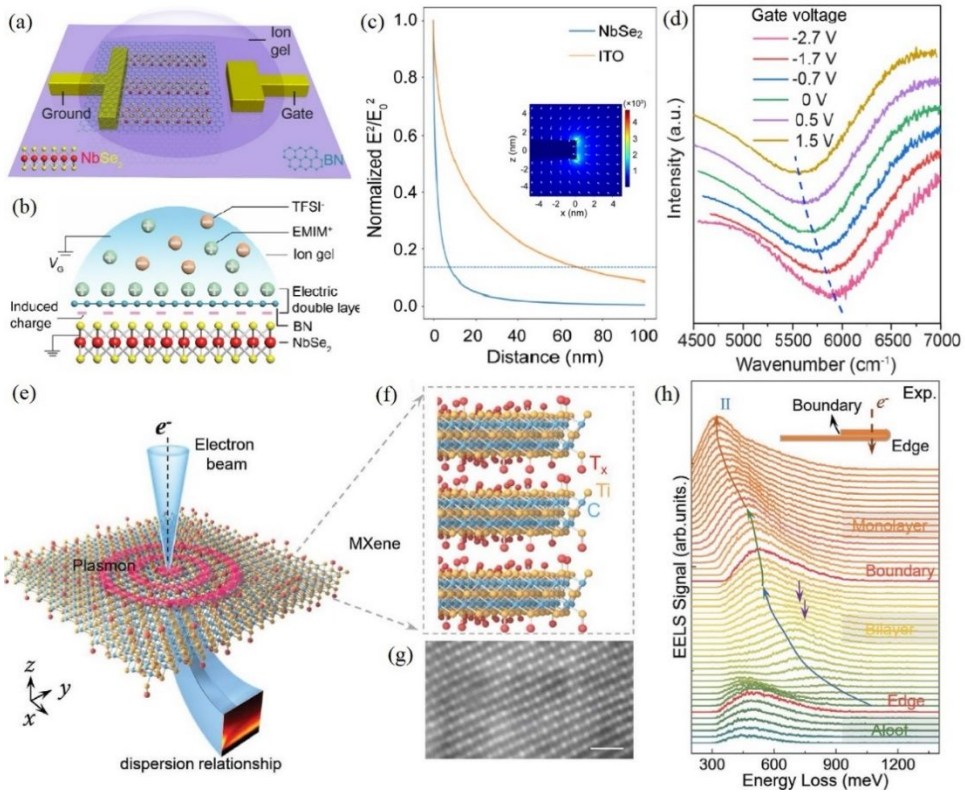

Figure 6. Tunable 2D plasmon polaritons in near-IR (a) Measurement configurations of tunable $NbSe_2$ plasmonics. **(b)** Electrostatic induced gating principle using ion gel. **(c)** The normalized electric field intensity as a function of the distance from the surface of $NbSe_2$ and ITO nanoribbons. **(d)** Tunable plasmonic resonance with varying gate voltage. **(e)** Schematic diagram of electron-excited MXene plasmon via EELS. **(f)** Diagram of the lattice structure and the chemical compositions of MXene. **(g)** High-angle annular dark-field transmission electron microscopy image of MXene film. **(h)** Experimental EELS spectra in MXene film. Figure 6(a) - 6(d) reproduced with permission from [91] © 2021 – Wiley, Figure 6(e) - 6(h) reproduced with permission from [92] © 2022 – AAAS.

Due to the relatively low carrier density (~10^{17} m^{-2}), graphene and BP are primarily active as highly tunable platforms in the mid-and far-IR range. Fortunately, the diversity of 2D materials makes it feasible to further push tunable plasmon into near-IR and even visible range. For example, as a boron analogue of graphene, borophene (a monolayer boron sheet) is an elemental 2D semi-metal that has been theoretically demonstrated to support tunable plasmon polaritons in the near-IR region due to its high density of Dirac electrons (~10^{19} m^{-2}) [93]. While there has been no experimental demonstration to date, several device concepts based on tunable borophene plasmon polaritons have been theoretically developed with impressive performance [94,95], offering

capabilities that are challenging to achieve with other materials. 2D metallic TMDCs like $NbSe_2$, NbS_2, and $TaSe_2$ [91,96,97], can also provide a promising strategy for realizing tunable plasmon polaritons in near-IR, which has been experimentally demonstrated recently. For example, M. Zhao *et al*. have reported that $NbSe_2$ supports electrostatic tunable plasmons in the near-IR region (Figure 6(a)-(b)), showing much tighter light confinement than the indium tin oxide (ITO) in this wavelength region (Figure 6(c)) [91]. By leveraging on the reduced charge screening effect of 2D semimetal and strong gating effect of ionic liquid, $NbSe_2$ plasmons can be actively tuned within a wide near-IR range, thus bridging the gap between graphene plasmon and conventional metal/doped semiconductor plasmon (Figure 6(d)). Recently, 2D metal carbides and nitrides (MXene) have also been demonstrated to support plasmon polaritons in near-IR regions [92,98]. Using high-spatial-resolution electron energy-loss spectroscopy (EELS), Guo et al. have characterized the plasmon dispersion of MXene films (Figure 6(e)-(h)). The MXene layer number and momentum are found to have a vital effect on the plasmon-induced electromagnetic absorption [92]. The vast library of van der Waals 2D materials provides a holistic platform for the realization of tunable plasmon polaritons across the spectral range from visible to mid-far-IR and THz, enabling tunable metaoptics that are previously unattainable with conventional plasmonic materials.

Tunable phonon polaritons

In contrast to plasmon polaritons, phonon polaritons (PhP) arising from phonon excitation are limited by phonon scattering loss instead of electronic losses. Hence, phonon polaritons have the potential to be low loss with strong field confinement by using crystals with high structural quality. h-BN was the first 2D material in which phonon polaritons were observed. Similarly, using s-SNOM, the real-space imaging of mid-IR phonon polaritons in h-BN has been achieved [39]. Compared with graphene plasmons, the phonon polaritons in h-BN show similar field confinement of $\lambda_{IR}/\lambda_p \sim 50$, where λ_{IR} is the incident IR light wavelength and λ_p is the phonon polariton wavelength, but with much longer propagation length up to 10 um than that for graphene plasmon (less than 1 um) [39]. While improving crystal quality is effective in reducing the damping of phonon polaritons, phonon scattering due to interfaces is still limiting the propagation length. To reduce phonon scattering by the substrate, h-BN on monocrystalline gold substrates[99] was developed to support phonon polaritons with twice longer propagation length compared with h-BN on SiO_2. By using isotope doping to modify the Reststrahlen band's dispersion, ultralow loss phonon polaritons

in isotopic h-BN have been observed, with a threefold improvement in polariton lifetime [100]. Nanopatterning has also been demonstrated to be an effective way to tune h-BN phonon polaritons. For example, ultra-confined resonances and strong field confinement of phonon polaritons have been demonstrated in h-BN planar nanostructures[101].

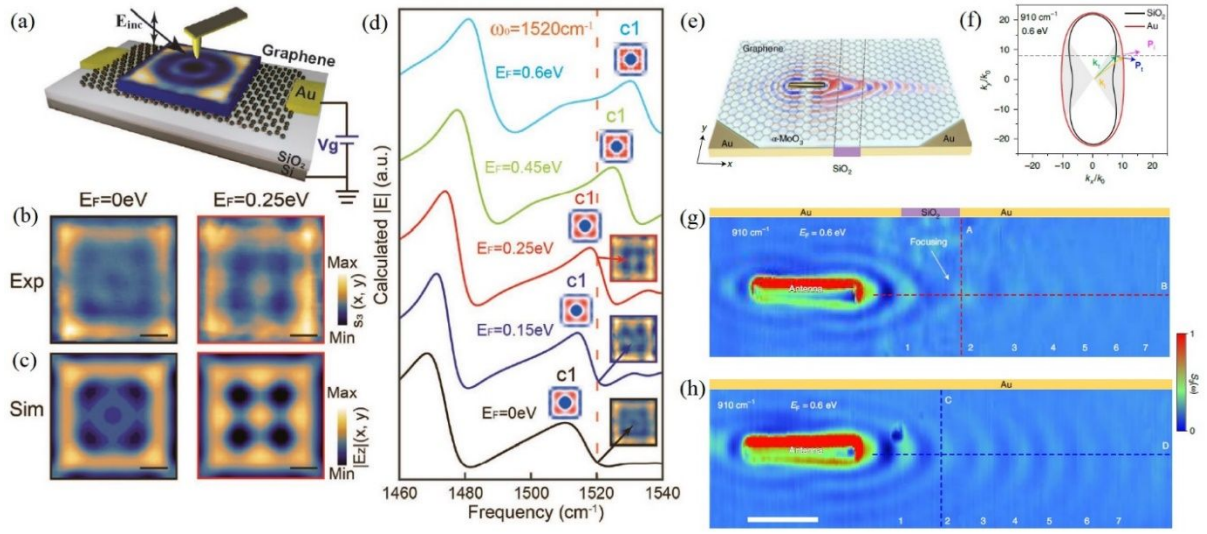

Figure 7. Tunable phonon polaritons. (a) Schematics of the s-SNOM measurements for gate-tuning phonon polaritons in a square h-BN nanoantenna. **(b)** Near-field images of phonon polaritons in a h-BN nanoantenna with different graphene Fermi levels. **(c)** Corresponding calculated images of phonon polaritons. **(d) Calculated** near-field mid-IR spectra of the h-BN nanoantenna with different graphene Fermi levels. **(e)** Schematic of the graphene/α-MoO_3 heterostructure on top of an Au-SiO_2-Au in-plane sandwich substrate. **(f)** Isofrequency hybrid polaritons dispersion contours for Au and SiO_2 substrates at 910 cm^{-1}. **(g)** Experimentally measured near-field amplitude image of hybrid polaritons showing partial focusing. **(h)** Experimentally measured hybrid phonon polaritons on a controlled Au substrate. Figure 7(a) - 7(d) reproduced from [103] with CC license, Figure 7(e) – (h) reproduced from [105] with CC license.

Although the insulating nature of h-BN makes its phonon polaritons incompatible with electrostatic control like that in graphene and $NbSe_2$, phonon polaritons in h-BN can be passively tuned with crystal thickness and tailoring the surrounding dielectric environment, in terms of both phonon polariton intensity and wavelength. Lately, by combining the merits of ultralow-loss phononics and active-tunable graphene plasmonics, *Duan et al*. observed the active tunable phonon polaritons in h-BN nanoantenna on top of a graphene layer (Figure 7(a)) [103]. The near-field

image experiences a significant change and the resonant spectral exhibits a clear shift as the graphene Fermi level varies, providing a concrete proof of an actively tunable h-BN phonon polariton (Figure 7(b)-(d)). The result suggests that combining h-BN nanoantennas with graphene not only reduces Ohmic losses in graphene plasmon but also preserves their active tunability, which paves the way for applications demanding tunable spectral selectivity and strong light-matter interaction.

α-MoO_3 recently has been another material of great interest for phonon polariton research. Real-space imaging has revealed that mid-IR phonon polariton in α-MoO_3 has comparable field confinement as graphene plasmon but a ten-time longer lifetime [102]. Moreover, phonon polariton in α-MoO_3 is in-plane anisotropic, with different wavelengths and dispersion along different in-plane crystalline orientations. Topological phase transition has been observed in the phonon polariton of twisted α-MoO_3 [104,106]. As the interlayer twist angle varies, the dispersion contours of phonon polariton can be altered from hyperbolic to elliptical. The hybridization of phonon polariton modifies the dispersion lines and accordingly, the anti-crossing of dispersion lines as well. It has been found that the twist angle-controlled transition is dedicated by a topological quantity, i.e., the number of anti-crossing points of the dispersion relation in reciprocal space [104]. Similar to the h-BN phonon polariton, image phonon polariton has also been observed for α-MoO_3 on metal surfaces, with enhanced propagation lifetime due to negligible substrate-mediated loss [107]. In terms of confinement, nanopatterns have been used to improve the quality factor of phonon polariton in α-MoO_3. Specifically, it has been shown that spatially confined freestanding α-MoO_3 on submicron-width trenches has a quality factor that is twice higher than those on flat substrates [108]. Combining with graphene, it is possible to actively tune the phonon polaritons in α-MoO_3. Recently, *Hu et al*. experimentally presented a topological transition in the isofrequency dispersion contours of hybrid polaritons with a graphene/α-MoO_3 (Figure 7(e)) heterostructure [105]. By changing the graphene Fermi levels, the contour topology transformed from open to closed shapes over a wide frequency range originating from the doping-dependent polariton hybridization. By further appropriately choosing the substrate, they managed to modify the dispersion contour to

achieve improved flatness, which allowed them to realize the sub-wavelength focusing of polaritons down to 4.8% of the free-space light wavelength through an in-plane lens made of 1.5-μm-wide silica substrate (Figure 7(f)-(h)).

Research in polaritons has made significant progress with the emergence of 2D materials. Regarding the active tuning of polaritons, a highly interesting but so far largely untouched direction is to utilize the rich topological and quantum properties associated with 2D materials as the knob to tune polaritons. The rich physics in 2D polaritonic materials, such as topological states in bilayer graphene [68], Ising superconductivity in $NbSe_2$ [69] and strong electron correlation in twisted graphene [109], makes it very appealing to establish connections between polaritons excitation and various physics. More interestingly, investigating different physics in one system is highly viable with 2D materials, and it is possible to open a new playground for polaritons studies and applications covering a wide spectral range from visible to terahertz.

Nonlinear metaoptics with 2D materials

Fundamentals of Nonlinear Metaoptics

Nonlinear metasurfaces have recently emerged as a promising platform to study the nonlinear optical phenomena in a planar system.[46] Realizing nonlinear phenomena such as wavelength conversion and switching in planar surfaces is important for optical information processing. In the earlier stage of development, plasmonic metasurfaces based on metallic sub-wavelength structures were employed to explore nonlinear phenomena due to the extreme sub-wavelength confinement of metallic elements and the possible nonlinear optical response of metals [110]. However, the thermal heating and high dissipative losses associated with plasmonic metasurfaces limit their wide applications. All-dielectric metasurfaces made of high refractive index materials have been proposed as an alternative for nonlinear metasurface development for their low loss and high damage threshold [43]. In addition to electronic nonlinear effects, the optically induced magnetic resonance supported by all-dielectric metasurfaces further enhances the nonlinear optical responses. Besides the well-known nonlinear phenomena such as harmonic generation and parametric frequency conversion, all-dielectric nonlinear metasurfaces can be used to realize other interesting nonlinear functionalities by using the underlying physics of Mie resonances [4] and the collective resonance such as guided mode resonance and optical bound states in the continuum

(BIC).[111] The new functionalities introduced by nonlinear metasurfaces include [45,112] asymmetric and chiral frequency conversion, multi-frequency and cascading effects, nonlinear quantum photonics and nonperturbative nonlinear regimes.

The second and third-order nonlinear processes such as second harmonic generation (SHG) and third harmonic generation (THG), respectively are the most common nonlinear optical effects. Even though these nonlinear effects are phase-sensitive, the required phase matching condition is not necessary in the metasurface due to its sub-wavelength scale dimension [112]. In particular, the light interaction happens at the sub-wavelength scale much smaller than the coherence length of the light. To realize an efficient nonlinear metasurface it requires [45]: (i) high nonlinear susceptibility value, (ii) large electromagnetic field enhancement at the resonances of metasurface and overlap of these resonances with fundamental and newly generated wave frequencies, and (iii) low loss of material at both the fundamental and newly generated wave frequencies. The field enhancement due to Mie-type resonance such as electric and magnetic dipole resonances, and anapole resonance at the fundamental frequency has been widely employed to boost the nonlinear process in all-dielectric metasurfaces [45,111,112]. In addition, high-quality factor BIC resonance realized in some metasurfaces can further enhance the nonlinear effects due to exceptionally high electromagnetic field enhancement at the fundamental frequency [45].

Nonlinear optical properties of 2D materials

In recent years, 2D materials and their hybrid structures have shown their great potential for nonlinear optics [46]. The first 2D material, graphene, exhibits a wide spectrum of nonlinear optical properties such as saturable absorption [113] (SA), THG [114], four-wave mixing [115] (FWM), self-phase modulation [116], coherent optical injection [117], optical limiting[118], and nonlinear Kerr effect [119]. The second-order nonlinear process such as SHG is not possible in graphene due to its centrosymmetric crystal structure. However, SHG has been realized at the interface of graphene/SiO2/Si systems by breaking the inversion symmetry [120,121]. Various physical and chemical methods have also been proposed for breaking the inversion symmetry [47,109,110]. The ability to tune the linear and nonlinear optical properties of graphene shows the key role of graphene in future reconfigurable optoelectronic devices.

TMDCs including MoS_2, $MoSe_2$, WS_2, and WSe_2 exhibit indirect-to-direct bandgap transition as their thickness is reduced from the bulk to the monolayer form and have shown fascinating linear

and nonlinear optical properties. By using both monolayer and few-layer TMDCs, nonlinear effects have been demonstrated including SA [122], SHG [123], THG [124], sum-and-difference frequency generation [125] (SFG), higher harmonic generation [126] (HHG), optical limiting [127] and FWM [128]. In contrast to graphene, second order and other even-order nonlinear processes can happen in TMDCs because they do not have inversion symmetry with an odd number of layers. The monolayer TMDC can provide large second order nonlinear susceptibilities in the range of 1 to 10^5 pm/V and the enhancement of SHG is due to the overlap of C-exciton resonance of TMDCs with the SHG wavelength [112]. This interesting feature is also useful for spintronic and valleytronic applications [129].

Many other 2D materials also exhibited interesting nonlinear optical properties. Compared to graphene and TMDCs, BP has been reported of significantly higher bandgap tunability of ~0.3eV to ~2.0 eV through crystal thickness manipulation [130]. In addition, BP is a suitable material for anisotropic optics because it has an anisotropic crystal structure. The nonlinear susceptibility of BP is high at $\sim 10^{-19}$ m^2 V^{-2} and has been utilized to realize THG [131], FWM [132], and SA [133]. However, the stability of BP is a limiting factor and proper encapsulation, or other methods are required to protect BP for long-term stability [134]. Moreover, other systems such as h-BN [135] and group III and IV metal chalcogenides [136] (GeSe and SnS) have also received wide interest. In Table 1, we summarized the nonlinear optical responses of different 2D materials [46].

2D material	Nonlinear effect[a]	Nonlinear coefficient[b]	Emission wavelength(nm)[c]	Thickness[d]
Graphene	THG	42000	263-1030	ML
	FWM	14000	360-1566	ML; FL
MoS_2	SHG	10000	370-780	ML; BL; FL
	THG	2.4	520-660	ML
	FWM	-	430-450	FL
$MoSe_2$	SHG	5	600-900	ML
	THG	2.2	520	ML
	FWM	-	750	ML
WS_2	SHG	900	415-660	ML
	THG	2.4	520	ML
WSe_2	SHG	1000	400-795	ML; BL
	THG	1	520	ML
GaSe	SHG	240	400-800	ML; FL
	THG	1600	520	FL
GaTe	SHG	0.115	760	7-57nm
	THG	2000	520	7-57nm
BP	THG	1.6	520	10nm; 1-4L
	FWM	-	1550	4.3nm; 18nm
$MoTe_2$	SHG	5	500	FL
ReS_2	THG	53	505	ML
InSe	SHG	-	530	9-25nm
hBN	SHG	200	405	ML; BL; FL

Table 1. **2D materials and their nonlinear optical responses**. [a]The most common nonlinear effects are highlighted. [b]Maximum achieved values of nonlinear coefficient are reported, for SHG, $\chi^{(2)} \times 10^{-11}$ m/V ; for THG and FWM, $\chi^{(3)} \times 10^{-19}$ m^2/V^2. [c]The spectral range of newly generated waves for SHG, THG and FWM are reported. [d]Thickness of 2D materials, ML=monolayer, BL=bilayer and FL=few-layers.

The hybrid structures of 2D materials are currently receiving significant attention to engineer their linear and nonlinear optical properties, where each 2D material layer can be smartly designed to control the desired functions independently [137]. With the advent of advanced growth and fabrication methods, the heterostructures of 2D materials can easily be fabricated by stacking different 2D materials. To date, various 2D material combinations including graphene–h-BN, –BP, TMDC–BN, –BP, –graphene, and TMDC–TMDC have been utilized to realize 2D heterostructures for numerous photonics applications [49]. In these structures, the nonlinear effects can be enhanced by the coherent superposition of the optical fields from the individual layers. So far, nonlinear effects such as SHG [138] and SA [139] have been demonstrated using 2D heterostructures. The design of a proper heterostructure superlattice is required to explore the other higher-order nonlinear effects.

Nonlinear metasurfaces based on 2D materials

Metasurfaces based on 2D materials have the advantages of high refractive index, ultrathin thickness, tunable feature, high-Q resonance and enhanced nonlinear response [140, 141–147]. Significant nonlinear effects were observed in 2D metasurfaces compared to monolayer and few-layers of 2D materials alone. Popkova *et al*. reported nonlinear exciton-Mie resonance coupling and second-order nonlinear effects using bulk MoS_2 [141]. As shown in Figure 8(a) – (d), nanodisks were fabricated on a thick flake of MoS_2 and achieved 23-fold enhancement of SHG compared to an unpatterned monolayer of MoS_2 for a fundamental wavelength of 900 nm. Here, the metasurface was carefully designed to excite the Mie-type resonance at 900 nm wavelength and to overlap the second harmonics wavelength at C-exciton resonance of MoS_2 (450 nm), and as a result, huge field enhancement was achieved at both the fundamental and newly generated wave frequencies. The observed enhanced SHG is also due to the anisotropic nature of fabricated nanodisks, which originated from the hexagonal crystalline structure.

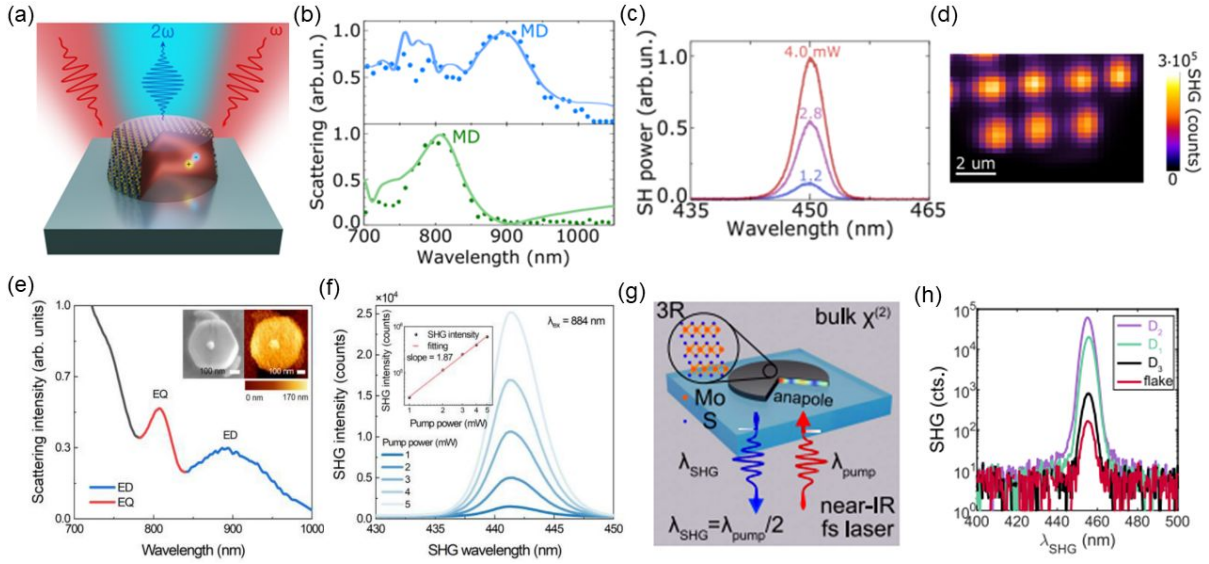

Figure 8. SHG from MoS_2 (a) Schematic representation of the SHG using MoS_2 nanodisks. **(b)** Measured (dot) and calculated (curve) scattering spectra of MoS_2 nanodisk metasurface for different disk diameters (550 nm for blue and 300 nm for green). **(c)** Measured second harmonic signal from a single nanodisk for different pump powers. **(d)** Mapping of second harmonic intensity over the nanodisk array at a pump wavelength of 900 nm. **(e)** Measured scattering spectrum from a MoS_2 nanoparticle. **(f)** Measured second harmonic signal from a MoS_2 nanoparticle shown in the inset of (e) for different pump power at a wavelength of 884 nm. **(g)** Schematic representation of the SHG in 3R-MoS_2 nanodisks. **(h)** Measured second harmonic spectrum of 3R-MoS_2 nanodisks with different disk diameters at a pump wavelength of

910 nm. Figure 8(a) – (d) reproduced with permission from [141] © 2022 – Wiley, Figure 8(e) and 8(f) reproduced with permission from [142] © 2023 – Wiley, Figure 8(g) and 8(h) reproduced from [143] with CC license.

A similar kind of result was reported by Panmai *et al*. [142], where the authors fabricated hexagonal-prism-like nanostructures in a thick flake of MoS_2. The Mie resonance was excited at the near-infrared wavelengths and the second harmonic wave was generated around the C-exciton resonance of MoS_2 (Fig. 8(e) and 8(f)). The authors also discussed the importance of the mode profile to enhance the nonlinear optical effects in TMDCs-metasurfaces, as they observed enhanced and suppressed SHG at electric dipole and electric quadrupole resonance, respectively. In a very recent paper [143], authors reported >100-fold enhancement of SHG from a single MoS_2 nanodisk patterned on a 3R phase MoS_2 multilayer (Fig. 8(g) and 8(h)). Note that the patterned 3R-MoS_2 nanodisk excites non-radiating Mie resonance such as anapole resonance and the reported >100-fold enhancement is obtained by comparing it with unpatterned MoS_2 multilayer. The anapole resonance and MoS_2 disk were further employed to realize enhanced third-order nonlinear effects such as FWM [144]. Compared to unpatterned MoS_2 flakes, an enhancement factor of 150 times at 1470 nm pump wavelength was realized by using a 3R-MoS_2 disk with a diameter and thickness of 1.62 μm and 108 nm, respectively.

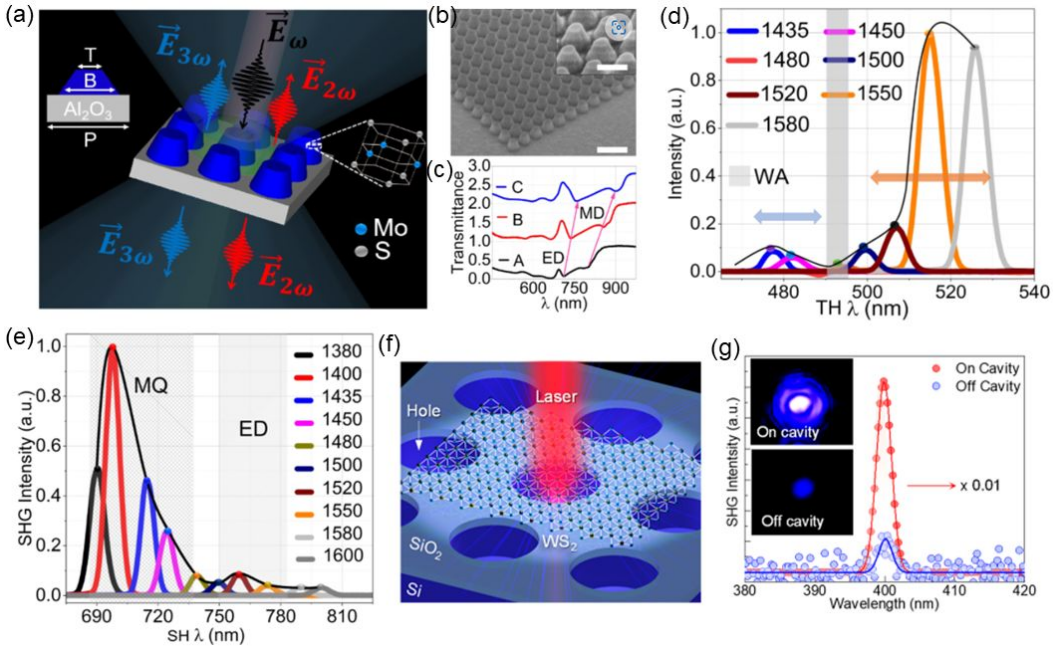

Figure 9. HHG from TMD metasurfaces (a) Concept of unidirectional SHG and THG using MoS_2 truncated cone metasurface. **(b)** SEM image of the fabricated metasurface. **(c)** Measured transmission spectra of metasurface with different structural parameters. Measured wavelength-dependent generation of **(d)** THG and **(e)** SHG from the metasurface. **(f)** Schematic of WS_2 monolayer on a F-P microcavity. **(g)** Measured second harmonic intensity from the On and Off cavity at an excitation wavelength of 800 nm. Figure 9(a) – (e) reproduced from [134] under CC license, Figure 9(f) and 9(g) reproduced with permission from [12] © 2022 – ACS.

Even though the nonlinear metasurfaces operate at a sub-diffraction regime for the fundamental wave, the emission of multiple diffractive beams at the nonlinearly generated harmonics restricts directional emission from such metasurfaces. This issue was addressed in a recent paper by Nauman *et al*. [145], in which the authors used a Mie resonant metasurface made up of truncated cones of MoS_2 (Fig. 9(a) – (c)). Through exploiting the extremely high refractive index of MoS_2, the unidirectional emission of SHG and THG with tunable SHG emission in forward and backward directions was realized (Fig. 9(d) and 9(e)). Along the same direction, Shi *et al.* [146] proposed a Fabry Pérot micro-cavity coupled monolayer WS_2 platform for direction and enhanced SHG (Fig. 9(f) and 9(g)). The strong electric field enhancement at the resonance of the microcavity benefited the enhanced and directional emission of SHG (diverging angle of ∼5°). Du *et al*. also demonstrated directional SHG emission using a heterostructure of MoS_2/WS_2 monolayer, which was suspended on a holey SiO_2/Si substrate[147] .

The aforementioned nonlinear metasurfaces have mainly been used to investigate the common nonlinear optical effects such as SHG and THG through exploiting the physics of Mie-resonance. However, the excitation of high-Q resonances at the fundamental wave frequencies is important to further improve the efficiency of second and third-order nonlinear effects and to generate higher-order nonlinear processes. Kühner *et al*. [148] experimentally demonstrated high-Q resonance such as quasi-BIC using h-BN metasurface. Although h-BN is a low refractive index dielectric, authors showcased symmetry-broken quasi-BIC resonance with a Q-factor > 300 over a spectral band from 400 nm to 1000 nm by fabricating the slit array metasurface on a single h-BN flake (Figure10(a) and 10(b)). By utilizing the enhanced electric near-field distribution at the quasi-BIC resonance, a 388-fold second harmonic enhancement factor in the ultraviolet wavelength was reported (Figure. 10(c)) [148]. There are also a few experimental reports on the realization of quasi-BIC resonance by

integrating TMDCs with all-dielectric metasurfaces for boosting the second-order nonlinear processes [149–152].

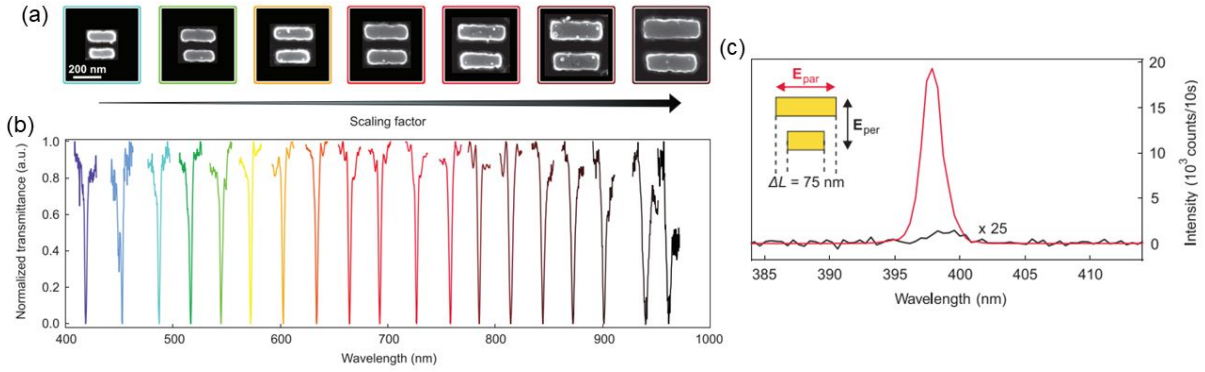

Figure 10. Quasi-BIC h-BN metasurface (a) SEM images of the fabricated metasurface unit cell on h-BN with increasing scaling factor and (b) the corresponding excited high-Q quasi-BIC resonance from 400 to 100 nm with increasing scaling factor. (c) The measured second harmonic signal from quasi-BIC metasurface. Figure 10 is reproduced with permission from [148] © 2023 – Wiley.

Since the main challenges associated with nonlinear optics in all-dielectric metasurfaces in the shorter wavelengths (visible and near IR) are the relatively low refractive index, large mode volumes, and low nonlinear response, the development of novel 2D materials-based nonlinear metasurfaces using the existing advanced techniques of growth, fabrication, and nanopatterning will have a significant impact in this field. Another important aspect of 2D materials is the high tunability of all 2D- and hybrid 2D- material based nonlinear metasurfaces, as it would allow the efficient spatial and temporal control of light for diverse nonlinear applications. In addition, the tunability feature enables us to realize nonlinear metasurfaces with full all-optical control over the transient behavior of nonlinear response at possibly a switching speed of femtoseconds [131], which is useful for next-generation high-speed data processing. We expect continued interest in this direction to realize other interesting nonlinear effects such as nonlinear quantum photonics, multi-frequency effects, cascaded harmonic generation, and asymmetric frequency conversion. The recently demonstrated concept of Mie voids [153], which has the low-index voids surrounded by a high-index dielectric, and thus the localized mode confines the light in air, provides another avenue for the realization of novel 2D material-based resonant metasurfaces with exceptionally high nonlinearities at the nanoscale for the shorter wavelengths.

Discussions

From the practical application point of view, 2D-material-based tunable metasurfaces can be used to develop ultra-sensitive label-free biosensors[79], ultra-thin metalenses[24,154–156] and meta-holograms[157,158] , and ultrathin and integrable light sources[154]. In particular, the electrically tunable plasmonic resonance of graphene in the infrared wavelength can be used for infrared spectroscopy to identify the vibrational fingerprints of different biomolecules[79]. Using the tunable feature of the sensor, multiplexed detection is possible by dynamically tuning the spectral positions of the graphene plasmons in a wide spectral band. In addition, flexible photonic devices can also be developed with 2D materials since they can be easily transferred to flexible materials and substrates, where strain-induced tuning can also be considered as an alternative tuning mechanism.

However, 2D materials still face the concern of stability in practical application. Compared to conventional bulk materials, many 2D materials exhibit susceptibility to the ambient environment [159]. Typically, the degradation arises from their intrinsic instability and atomic-level defects induced by external factors such as oxygen and water adsorption and light illumination [160–162]. Encapsulation is the primary strategy to stabilize 2D materials [163]. One way is using a protective layer, such as hBN [164,165], atomic layer deposited high-k dielectrics[166,167] or polymer capping [168,169] to isolate 2D materials from the environment directly. The other way is functionalizing 2D materials with organic or inorganic substances to inert their surface [170,171]. These two ways can also be combined to further ensure the stability of 2D materials-based devices.

Furthermore, a careful selection of 2D material preparation techniques is required to optimize the metaoptics performance. Direct synthesis, also known as the bottom-up method, such as the chemical vapour deposition, allows controlled growth of 2D materials on substrates, offering large-area growth[172], high scalability and precise control over layer thickness[173], but simultaneously facing the shortcoming of being substrate-sensitive and requiring high temperature[174]. On the other hand, exfoliation from bulk crystals, also known as the top-down method, promises high-quality flakes, with the drawback of miniature flake sizes[175–177]. This technique includes mechanical exfoliation, liquid-phase exfoliation and more recently electrochemical exfoliation. A summary of the key features of the exfoliation methods is presented in Table 2a. Moreover, in producing tunable metaoptics, it is noteworthy that nanopatterning of 2D materials is a crucial technique[178,179], with the top-down approach being the primary method. Various common top-down approaches, ranking from the highest to the lowest in patterning

resolution, include lithography and etching[24,37,60,62], tip or ion-assisted direct patterning[22,26] and optical direct-pattern[23], all bear their respective merits and drawbacks that warrant deliberate consideration for performance optimization. A list of the common techniques discussed in this review is summarized in Table 2b.

(a)

Method	**Typical Size**	**Key Features**	**Pros**	**Cons**	**Ref**
Mechanical Exfoliation	nm - μm	Use adhesive tapes to delaminate bulk materials, ideal for research	High-quality flakes, preserving material intrinsic properties	Limited scalability, labour intensive and miniature flake sizes	175 – 177
Liquid-phase Exfoliation	nm - μm	Use adhesive tapes to delaminate bulk materials, ideal for scalable production	High versatility and scalability	Reduced flake quality from solvent residue	180 – 182
Electrochemical Exfoliation	Up to hundreds of μm	Use Electric fields to exfoliate materials either in solution or on electrodes, ideal for device fabrication	Large size samples, high scalability and tunability, limited environmental impact	Limited throughput	91, 183, 184

(b)

Method	**Feature Size**	**Key Features**	**Pros**	**Cons**	**Ref**
Lithography (UV & DUV, e-beam) and Etching	From μm to 10 nm	Pattern creation via lithography and etching, can achieve high resolution and integration.	Compatible with existing semiconductor processes; high precision.	Potential damage from etching processes; photoresist residues.	24, 37, 60, 62
Tip or Ion Assisted Direct-Patterning	Sub-100 nm	Direct pattern writing with tip or ion offers customization and clean surfaces.	Avoids photoresist residues; enables customized patterning.	Generally slower process; higher cost for high-resolution patterns.	22, 26
Optical Direct-Patterning	Down to 100 nm	Direct pattern writing by high power laser offers customization and clean surfaces.	Avoids photoresist residues; enables customized patterning.	Lower resolution comparing to the other two methods	23

Table 2. 2D Materials Preparation Methods. We summarize the key features for the common top-down approaches in 2D materials preparation for (a) exfoliation and (b) nano-patterning.

Conclusion

In this review, we focused on the current rising research interest in tunable 2D material-based metaoptics to provide a detailed coverage of the progress, challenges, and prospects of this area. We introduced the channels to enable tunability in 2D systems including excitons, trions, plasmon and phonon polaritons, and then discussed the recent advancements in the nonlinear metaoptics made of 2D materials.

First, we highlighted the promises of excitons and trions as the knobs to achieve the tunability of metaoptics. We showcased the uniqueness of these quasiparticles in the 2D system and discussed how their strong and controllable resonances enable state-of-the-art 2D material-based tunable metaoptics. The specific challenges faced in this direction and the needs to be addressed by the community are also assessed like uniform electrostatic gating across a large 2D sample in the future and broadband excitonic tunability.

Second, 2D polaritons are discussed, which offer another avenue to enable large tunability 2D metaoptics with strong light matter interaction. 2D plasmon polaritons in semimetals cover a wide spectral range from far to near IR, while 2D phonon polaritons in both h-BN and α-MoO3 have a significantly longer lifetime and the potential to improve the quality factor of the metaoptics, which could see more applications in like nonlinear optics and quantum photonics. s-SNOM is particularly a powerful tool in direct visualization and manipulation of polaritons in 2D metaoptics. Further understanding of the nontrivial tip-sample interaction and spatial-temporal s-SNOM measurement would greatly benefit the 2D metaoptics and 2D materials study in general.

Finally, we presented the 2D nonlinear metaoptics in which 2D materials and their hybrid structures are used either as the nonlinear media or metaoptics themselves. Various nonlinear effects including SHG and HHG with good efficiency and high-quality factors have been demonstrated to address the shortcomings of all-dielectric metasurfaces. The tunable nonlinear metasurfaces using all-2D materials are yet to emerge and would be an interesting direction to explore.

The unique properties possessed by various 2D materials, such as high refractive index, tunable exciton and polariton resonance by gate voltage, forming Moiré superlattice, strong interlayer coupling, van der Waals nature for easy integration with various substrates and constructing heterostructures, rich of choices of materials in semiconductor, semimetal, ferroelectric, ferromagnetic, large nonlinear coefficient, etc. make 2D system a promising platform for tunable and nonlinear metaoptics. Further fundamental studies of physics and materials, and technological advancements in material growth, stacking and nanofabrication would unleash the full potential of 2D tunable and nonlinear metaoptics to benefit photonics-in-general development.

Acknowledgement:

This work is financially supported by the National Research Foundation Singapore under CRP program (Grant No. NRF-CRP26-2021-0004), A*STAR (Agency for Science, Technology and Research) under AME IRG Program (Grant No. A2083c0058 and A20E5c0084), MTC Program (Grant No. M22L1b0110) and HBMS IAF-PP (Grant No. H19H6a0025).

Competing interests

The authors declare no competing financial interests.

References:

1. Smith, D. R., Pendry, J. B. & Wiltshire, M. C. K. Metamaterials and Negative Refractive Index. *Science* **305**, 788–792 (2004).
2. Staude, I. & Schilling, J. Metamaterial-inspired silicon nanophotonics. *Nat. Photonics* **11**, 274–284 (2017).
3. Jahani, S. & Jacob, Z. All-dielectric metamaterials. *Nat. Nanotechnol.* **11**, 23–36 (2016).
4. Yu, N. & Capasso, F. Flat optics with designer metasurfaces. *Nat. Mater.* **13**, 139–150 (2014).
5. Shaltout, A. M., Shalaev, V. M. & Brongersma, M. L. Spatiotemporal light control with active metasurfaces. *Science* **364**, eaat3100 (2019).

6. Park, J. *et al.* All-solid-state spatial light modulator with independent phase and amplitude control for three-dimensional LiDAR applications. *Nat. Nanotechnol.* **16**, 69–76 (2021).

7. Babicheva, V. E., Boltasseva, A. & Lavrinenko, A. V. Transparent conducting oxides for electro-optical plasmonic modulators. *Nanophotonics* **4**, 165–185 (2015).

8. Wang, Z. *et al.* A Novel Chiral Metasurface with Controllable Circular Dichroism Induced by Coupling Localized and Propagating Modes. *Adv. Opt. Mater.* **4**, 883–888 (2016).

9. Enkrich, C. *et al.* Magnetic Metamaterials at Telecommunication and Visible Frequencies. *Phys. Rev. Lett.* **95**, 203901 (2005).

10. Zhao, Q., Zhou, J., Zhang, F. & Lippens, D. Mie resonance-based dielectric metamaterials. *Mater. Today* **12**, 60–69 (2009).

11. Nemati, A., Wang, Q., Hong, M. & Teng, J. Tunable and reconfigurable metasurfaces and metadevices. *Opto-Electron. Adv.* **1**, 180009–25 (2018).

12. Abdelraouf, O. A. M. *et al.* Recent Advances in Tunable Metasurfaces: Materials, Design, and Applications. *ACS Nano* **16**, 13339–13369 (2022).

13. Buchnev, O., Podoliak, N., Kaczmarek, M., Zheludev, N. I. & Fedotov, V. A. Electrically Controlled Nanostructured Metasurface Loaded with Liquid Crystal: Toward Multifunctional Photonic Switch. *Adv. Opt. Mater.* **3**, 674–679 (2015).

14. Badloe, T. *et al.* Liquid crystal-powered Mie resonators for electrically tunable photorealistic color gradients and dark blacks. *Light Sci. Appl.* **11**, 118 (2022).

15. Li, S.-Q. *et al.* Phase-only transmissive spatial light modulator based on tunable dielectric metasurface. *Science* **364**, 1087–1090 (2019).

16. Zheng, C. *et al.* Enabling Active Nanotechnologies by Phase Transition: From Electronics, Photonics to Thermotics. *Chem. Rev.* **122**, 15450–15500 (2022).

17. Lepeshov, S. & Krasnok, A. Tunable phase-change metasurfaces. *Nat. Nanotechnol.* **16**, 615–616 (2021).

18. Zhang, Y. *et al.* Electrically reconfigurable non-volatile metasurface using low-loss optical phase-change material. *Nat. Nanotechnol.* **16**, 661–666 (2021).

19. Wang, Y. *et al.* Electrical tuning of phase-change antennas and metasurfaces. *Nat. Nanotechnol.* **16**, 667–672 (2021).

20. Wang, G. *et al.* Colloquium: Excitons in atomically thin transition metal dichalcogenides. *Rev. Mod. Phys.* **90**, 021001 (2018).

21. Mas-Ballesté, R., Gómez-Navarro, C., Gómez-Herrero, J. & Zamora, F. 2D materials: to graphene and beyond. *Nanoscale* **3**, 20–30 (2011).

22. Wang, Z. *et al.* Exciton-Enabled Meta-Optics in Two-Dimensional Transition Metal Dichalcogenides. *Nano Lett.* **20**, 7964–7972 (2020).

23. Wang, Y. *et al.* Atomically Thin Noble Metal Dichalcogenides for Phase-Regulated Meta-optics. *Nano Lett.* **20**, 7811–7818 (2020).

24. Liu, C.-H. *et al.* Ultrathin van der Waals Metalenses. *Nano Lett.* **18**, 6961–6966 (2018).

25. Rodin, A., Trushin, M., Carvalho, A. & Castro Neto, A. H. Collective excitations in 2D materials. *Nat. Rev. Phys.* **2**, 524–537 (2020).

26. Dasgupta, A., Gao, J. & Yang, X. Atomically Thin Nonlinear Transition Metal Dichalcogenide Holograms. *Nano Lett.* **19**, 6511–6516 (2019).

27. Yu, Y. *et al.* Giant Gating Tunability of Optical Refractive Index in Transition Metal Dichalcogenide Monolayers. *Nano Lett.* **17**, 3613–3618 (2017).

28. Li, M., Biswas, S., Hail, C. U. & Atwater, H. A. Refractive Index Modulation in Monolayer Molybdenum Diselenide. *Nano Lett.* **21**, 7602–7608 (2021).

29. Mak, K. F. *et al.* Tightly bound trions in monolayer MoS2. *Nat. Mater.* **12**, 207–211 (2013).

30. Chen, P. *et al.* Approaching the intrinsic exciton physics limit in two-dimensional semiconductor diodes. *Nature* **599**, 404–410 (2021).

31. Lien, D.-H. *et al.* Electrical suppression of all nonradiative recombination pathways in monolayer semiconductors. *Science* **364**, 468–471 (2019).

32. Harats, M. G., Kirchhof, J. N., Qiao, M., Greben, K. & Bolotin, K. I. Dynamics and efficient conversion of excitons to trions in non-uniformly strained monolayer WS2. *Nat. Photonics* **14**, 324–329 (2020).

33. Ross, J. S. *et al.* Electrical control of neutral and charged excitons in a monolayer semiconductor. *Nat. Commun.* **4**, 1474 (2013).

34. Zhang, Q. *et al.* Simultaneous capturing phonon and electron dynamics in MXenes. *Nat. Commun.* **13**, 7900 (2022).

35. Grigorenko, A. N., Polini, M. & Novoselov, K. S. Graphene plasmonics. *Nat. Photonics* **6**, 749–758 (2012).

36. Sebek, M. *et al.* Hybrid Plasmonics and Two-Dimensional Materials: Theory and Applications. *J. Mol. Eng. Mater.* **08**, 2030001 (2020).

37. Li, P. *et al.* Infrared hyperbolic metasurface based on nanostructured van der Waals materials. *Science* **359**, 892–896 (2018).

38. Elbanna, A. *et al.* 2D Material Infrared Photonics and Plasmonics. *ACS Nano* **17**, 4134–4179 (2023).

39. Dai, S. *et al.* Tunable Phonon Polaritons in Atomically Thin van der Waals Crystals of Boron Nitride. *Science* **343**, 1125–1129 (2014).

40. Krasnok, A., Tymchenko, M. & Alù, A. Nonlinear metasurfaces: a paradigm shift in nonlinear optics. *Mater. Today* **21**, 8–21 (2018).

41. Huang, T. *et al.* Planar nonlinear metasurface optics and their applications. *Rep. Prog. Phys.* **83**, 126101 (2020).

42. Rahimi, E. & Gordon, R. Nonlinear Plasmonic Metasurfaces. *Adv. Opt. Mater.* **6**, 1800274 (2018).

43. Sain, B., Meier, C. & Zentgraf, T. Nonlinear optics in all-dielectric nanoantennas and metasurfaces: a review. *Adv. Photonics* **1**, 024002 (2019).

44. Grinblat, G. Nonlinear Dielectric Nanoantennas and Metasurfaces: Frequency Conversion and Wavefront Control. *ACS Photonics* **8**, 3406–3432 (2021).

45. Pertsch, T. & Kivshar, Y. Nonlinear optics with resonant metasurfaces. *MRS Bull.* **45**, 210–220 (2020).

46. Autere, A. *et al.* Nonlinear Optics with 2D Layered Materials. *Adv. Mater.* **30**, 1705963 (2018).

47. Jiang, T. *et al.* Gate-tunable third-order nonlinear optical response of massless Dirac fermions in graphene. *Nat. Photonics* **12**, 430–436 (2018).

48. Huang, B. *et al.* Tuning inelastic light scattering via symmetry control in the two-dimensional magnet CrI3. *Nat. Nanotechnol.* **15**, 212–216 (2020).

49. Sun, Z., Martinez, A. & Wang, F. Optical modulators with 2D layered materials. *Nat. Photonics* **10**, 227–238 (2016).

50. Wang, G. *et al.* Giant Enhancement of the Optical Second-Harmonic Emission of WSe2 Monolayers by Laser Excitation at Exciton Resonances. *Phys. Rev. Lett.* **114**, 097403 (2015).

51. Chernikov, A. *et al.* Exciton Binding Energy and Nonhydrogenic Rydberg Series in Monolayer WS2. *Phys. Rev. Lett.* **113**, 076802 (2014).

52. Lynch, J., Guarneri, L., Jariwala, D. & van de Groep, J. Exciton resonances for atomically-thin optics. *J. Appl. Phys.* **132**, 091102 (2022).

53. Arora, A. *et al.* Excited-State Trions in Monolayer WS2. *Phys. Rev. Lett.* **123**, 167401 (2019).

54. Wang, Z. *et al.* Greatly Enhanced Resonant Exciton-Trion Conversion in Electrically Modulated Atomically Thin WS2 at Room Temperature. *Adv. Mater.* **35**, 2302248 (2023).

55. Lee, M.-J. *et al.* Measurement of Exciton and Trion Energies in Multistacked hBN/WS2 Coupled Quantum Wells for Resonant Tunneling Diodes. *ACS Nano* **14**, 16114–16121 (2020).

56. Goldstein, T. *et al.* Ground and excited state exciton polarons in monolayer MoSe2. *J. Chem. Phys.* **153**, 071101 (2020).

57. Wagner, K. *et al.* Autoionization and Dressing of Excited Excitons by Free Carriers in Monolayer WSe2. *Phys. Rev. Lett.* **125**, 267401 (2020).

58. Chernikov, A. *et al.* Electrical Tuning of Exciton Binding Energies in Monolayer WS2. *Phys. Rev. Lett.* **115**, 126802 (2015).

59. Back, P., Zeytinoglu, S., Ijaz, A., Kroner, M. & Imamoğlu, A. Realization of an Electrically Tunable Narrow-Bandwidth Atomically Thin Mirror Using Monolayer MoSe2. *Phys. Rev. Lett.* **120**, 037401 (2018).

60. Li, M., Hail, C. U., Biswas, S. & Atwater, H. A. Excitonic Beam Steering in an Active van der Waals Metasurface. *Nano Lett.* **23**, 2771–2777 (2023).

61. Zhou, Y. *et al.* Controlling Excitons in an Atomically Thin Membrane with a Mirror. *Phys. Rev. Lett.* **124**, 027401 (2020).

62. van de Groep, J. *et al.* Exciton resonance tuning of an atomically thin lens. *Nat. Photonics* **14**, 426–430 (2020).

63. Li, Q. *et al.* A Purcell-enabled monolayer semiconductor free-space optical modulator. *Nat. Photonics* **17**, 897–903 (2023).

64. Low, T. *et al.* Polaritons in layered two-dimensional materials. *Nat. Mater.* **16**, 182–194 (2017).

65. Xu, Q. *et al.* Meta-optics inspired surface plasmon devices. *Photonics Insights* **2**, R02–R02 (2023).

66. Xia, F., Wang, H., Xiao, D., Dubey, M. & Ramasubramaniam, A. Two-dimensional material nanophotonics. *Nat. Photonics* **8**, 899–907 (2014).

67. Xin, H., Namgung, B. & Lee, L. P. Nanoplasmonic optical antennas for life sciences and medicine. *Nat. Rev. Mater.* **3**, 228–243 (2018).

68. Jiang, N., Zhuo, X. & Wang, J. Active Plasmonics: Principles, Structures, and Applications. *Chem. Rev.* **118**, 3054–3099 (2018).

69. Zheludev, N. I. & Yuan, G. Optical superoscillation technologies beyond the diffraction limit. *Nat. Rev. Phys.* **4**, 16–32 (2022).

70. Koppens, F. H. L., Chang, D. E. & García de Abajo, F. J. Graphene Plasmonics: A Platform for Strong Light–Matter Interactions. *Nano Lett.* **11**, 3370–3377 (2011).

71. Fei, Z. *et al.* Gate-tuning of graphene plasmons revealed by infrared nano-imaging. *Nature* **487**, 82–85 (2012).

72. Chen, J. *et al.* Optical nano-imaging of gate-tunable graphene plasmons. *Nature* **487**, 77–81 (2012).

73. Wang, L. & Xu, X. G. Scattering-type scanning near-field optical microscopy with reconstruction of vertical interaction. *Nat. Commun.* **6**, 8973 (2015).

74. Woessner, A. *et al.* Highly confined low-loss plasmons in graphene–boron nitride heterostructures. *Nat. Mater.* **14**, 421–425 (2015).

75. Ni, G. X. *et al.* Fundamental limits to graphene plasmonics. *Nature* **557**, 530–533 (2018).

76. Nong, J. *et al.* Enhanced Graphene Plasmonic Mode Energy for Highly Sensitive Molecular Fingerprint Retrieval. *Laser Photonics Rev.* **15**, 2000300 (2021).

77. Fang, Z. *et al.* Active Tunable Absorption Enhancement with Graphene Nanodisk Arrays. *Nano Lett.* **14**, 299–304 (2014).

78. Rodrigo, D. *et al.* Double-layer graphene for enhanced tunable infrared plasmonics. *Light Sci. Appl.* **6**, e16277–e16277 (2017).

79. Yan, H. *et al.* Damping pathways of mid-infrared plasmons in graphene nanostructures. *Nat. Photonics* **7**, 394–399 (2013).

80. Brar, V. W. *et al.* Electronic modulation of infrared radiation in graphene plasmonic resonators. *Nat. Commun.* **6**, 7032 (2015).

81. Kim, S. *et al.* Electronically tunable extraordinary optical transmission in graphene plasmonic ribbons coupled to subwavelength metallic slit arrays. *Nat. Commun.* **7**, 12323 (2016).

82. Rodrigo, D. *et al.* Mid-infrared plasmonic biosensing with graphene. *Science* **349**, 165–168 (2015).

83. Hu, H. *et al.* Far-field nanoscale infrared spectroscopy of vibrational fingerprints of molecules with graphene plasmons. *Nat. Commun.* **7**, 12334 (2016).

84. Guo, Q. *et al.* Efficient electrical detection of mid-infrared graphene plasmons at room temperature. *Nat. Mater.* **17**, 986–992 (2018).

85. Sun, T. *et al.* Graphene plasmonic nanoresonators/graphene heterostructures for efficient room-temperature infrared photodetection. *J. Semicond.* **41**, 072907 (2020).

86. Fei, Z. *et al.* Tunneling Plasmonics in Bilayer Graphene. *Nano Lett.* **15**, 4973–4978 (2015).

87. Huang, T. *et al.* Observation of chiral and slow plasmons in twisted bilayer graphene. *Nature* **605**, 63–68 (2022).

88. Zhang, S. *et al.* Visualizing moiré ferroelectricity via plasmons and nano-photocurrent in graphene/twisted-WSe2 structures. *Nat. Commun.* **14**, 6200 (2023).

89. Lee, I.-H. *et al.* Anisotropic Acoustic Plasmons in Black Phosphorus. *ACS Photonics* **5**, 2208–2216 (2018).

90. Huang, X. *et al.* Black Phosphorus Carbide as a Tunable Anisotropic Plasmonic Metasurface. *ACS Photonics* **5**, 3116–3123 (2018).

91. Zhao, M. *et al.* Electrostatically Tunable Near-Infrared Plasmonic Resonances in Solution-Processed Atomically Thin NbSe2. *Adv. Mater.* **33**, 2101950 (2021).

92. Guo, X. *et al.* Studying Plasmon Dispersion of MXene for Enhanced Electromagnetic Absorption. *Adv. Mater.* **34**, 2201120 (2022).

93. Lian, C. *et al.* Integrated Plasmonics: Broadband Dirac Plasmons in Borophene. *Phys. Rev. Lett.* **125**, 116802 (2020).

94. Nong, J., Feng, F., Min, C., Yuan, X. & Somekh, M. Effective Transmission Modulation at Telecommunication Wavelengths through Continuous Metal Films Using Coupling between Borophene Plasmons and Magnetic Polaritons. *Adv. Opt. Mater.* **9**, 2001809 (2021).

95. Nong, J. *et al.* Active Modulation of Graphene Near-Infrared Electroabsorption Employing Borophene Plasmons in a Wide Waveband. *Adv. Opt. Mater.* **10**, 2102131 (2022).

96. Song, C. *et al.* Plasmons in the van der Waals charge-density-wave material 2H-TaSe2. *Nat. Commun.* **12**, 386 (2021).

97. Cudazzo, P. *et al.* Negative plasmon dispersion in 2H-NbS2 beyond the charge-density-wave interpretation. *New J. Phys.* **18**, 103050 (2016).

98. Pacheco-Peña, V., Hallam, T. & Healy, N. MXene supported surface plasmons on telecommunications optical fibers. *Light Sci. Appl.* **11**, 22 (2022).

99. Menabde, S. G. *et al.* Near-field probing of image phonon-polaritons in hexagonal boron nitride on gold crystals. *Sci. Adv.* **8**, eabn0627 (2022).

100. Giles, A. J. *et al.* Ultralow-loss polaritons in isotopically pure boron nitride. *Nat. Mater.* **17**, 134–139 (2018).

101. Tamagnone, M. *et al.* Ultra-confined mid-infrared resonant phonon polaritons in van der Waals nanostructures. *Sci. Adv.* **4**, eaat7189 (2018).

102. Ma, W. *et al.* In-plane anisotropic and ultra-low-loss polaritons in a natural van der Waals crystal. *Nature* **562**, 557–562 (2018).

103. Duan, J. *et al.* Active and Passive Tuning of Ultranarrow Resonances in Polaritonic Nanoantennas. *Adv. Mater.* **34**, 2104954 (2022).

104. Hu, G. *et al.* Topological polaritons and photonic magic angles in twisted α-MoO3 bilayers. *Nature* **582**, 209–213 (2020).

105. Hu, H. *et al.* Doping-driven topological polaritons in graphene/α-MoO3 heterostructures. *Nat. Nanotechnol.* **17**, 940–946 (2022).

106. Chen, M. *et al.* Configurable phonon polaritons in twisted α-MoO3. *Nat. Mater.* **19**, 1307–1311 (2020).

107. Menabde, S. G. *et al.* Low-Loss Anisotropic Image Polaritons in van der Waals Crystal α-MoO3. *Adv. Opt. Mater.* **10**, 2201492 (2022).

108. Yang, J. *et al.* High-Q Phonon-polaritons in Spatially Confined Freestanding α-MoO3. *ACS Photonics* **9**, 905–913 (2022).

109. Cao, Y. *et al.* Correlated insulator behaviour at half-filling in magic-angle graphene superlattices. *Nature* **556**, 80–84 (2018).

110. Kauranen, M. & Zayats, A. V. Nonlinear plasmonics. *Nat. Photonics* **6**, 737–748 (2012).

111. Koshelev, K., Bogdanov, A. & Kivshar, Y. Meta-optics and bound states in the continuum. *Sci. Bull.* **64**, 836–842 (2019).

112. Vabishchevich, P. & Kivshar, Y. Nonlinear photonics with metasurfaces. *Photonics Res.* **11**, B50–B64 (2023).

113. Sun, Z., Hasan, T. & Ferrari, A. C. Ultrafast lasers mode-locked by nanotubes and graphene. *Phys. E Low-Dimens. Syst. Nanostructures* **44**, 1082–1091 (2012).

114. Säynätjoki, A. *et al.* Rapid Large-Area Multiphoton Microscopy for Characterization of Graphene. *ACS Nano* **7**, 8441–8446 (2013).

115. Hendry, E., Hale, P. J., Moger, J., Savchenko, A. K. & Mikhailov, S. A. Coherent Nonlinear Optical Response of Graphene. *Phys. Rev. Lett.* **105**, 097401 (2010).

116. Wu, R. *et al.* Purely Coherent Nonlinear Optical Response in Solution Dispersions of Graphene Sheets. *Nano Lett.* **11**, 5159–5164 (2011).

117. Sun, D. *et al.* Coherent Control of Ballistic Photocurrents in Multilayer Epitaxial Graphene Using Quantum Interference. *Nano Lett.* **10**, 1293–1296 (2010).

118. Wang, J., Hernandez, Y., Lotya, M., Coleman, J. N. & Blau, W. J. Broadband Nonlinear Optical Response of Graphene Dispersions. *Adv. Mater.* **21**, 2430–2435 (2009).

119. Yang, H. *et al.* Giant Two-Photon Absorption in Bilayer Graphene. *Nano Lett.* **11**, 2622–2627 (2011).

120. Dean, J. J. & van Driel, H. M. Second harmonic generation from graphene and graphitic films. *Appl. Phys. Lett.* **95**, 261910 (2009).

121. Dean, J. J. & van Driel, H. M. Graphene and few-layer graphite probed by second-harmonic generation: Theory and experiment. *Phys. Rev. B* **82**, 125411 (2010).

122. Wang, K. *et al.* Ultrafast Saturable Absorption of Two-Dimensional MoS2 Nanosheets. *ACS Nano* **7**, 9260–9267 (2013).

123. Li, Y. *et al.* Probing Symmetry Properties of Few-Layer MoS2 and h-BN by Optical Second-Harmonic Generation. *Nano Lett.* **13**, 3329–3333 (2013).

124. Säynätjoki, A. *et al.* Ultra-strong nonlinear optical processes and trigonal warping in MoS2 layers. *Nat. Commun.* **8**, 893 (2017).

125. Janisch, C. *et al.* Ultrashort optical pulse characterization using WS_2 monolayers. *Opt. Lett.* **39**, 383–385 (2014).

126. Liu, H. *et al.* High-harmonic generation from an atomically thin semiconductor. *Nat. Phys.* **13**, 262–265 (2017).

127. Dong, N. *et al.* Optical Limiting and Theoretical Modelling of Layered Transition Metal Dichalcogenide Nanosheets. *Sci. Rep.* **5**, 14646 (2015).

128. Jakubczyk, T. *et al.* Radiatively Limited Dephasing and Exciton Dynamics in MoSe2 Monolayers Revealed with Four-Wave Mixing Microscopy. *Nano Lett.* **16**, 5333–5339 (2016).

129. Xu, X., Yao, W., Xiao, D. & Heinz, T. F. Spin and pseudospins in layered transition metal dichalcogenides. *Nat. Phys.* **10**, 343–350 (2014).

130. Qiao, J., Kong, X., Hu, Z.-X., Yang, F. & Ji, W. High-mobility transport anisotropy and linear dichroism in few-layer black phosphorus. *Nat. Commun.* **5**, 4475 (2014).

131. Youngblood, N., Peng, R., Nemilentsau, A., Low, T. & Li, M. Layer-Tunable Third-Harmonic Generation in Multilayer Black Phosphorus. *ACS Photonics* **4**, 8–14 (2017).

132. Zheng, J. *et al.* Black Phosphorus Based All-Optical-Signal-Processing: Toward High Performances and Enhanced Stability. *ACS Photonics* **4**, 1466–1476 (2017).

133. Hu, G. *et al.* Black phosphorus ink formulation for inkjet printing of optoelectronics and photonics. *Nat. Commun.* **8**, 278 (2017).

134. Illarionov, Y. Y. *et al.* Long-Term Stability and Reliability of Black Phosphorus Field-Effect Transistors. *ACS Nano* **10**, 9543–9549 (2016).

135. Tran, T. T., Bray, K., Ford, M. J., Toth, M. & Aharonovich, I. Quantum emission from hexagonal boron nitride monolayers. *Nat. Nanotechnol.* **11**, 37–41 (2016).

136. Wang, H. & Qian, X. Giant Optical Second Harmonic Generation in Two-Dimensional Multiferroics. *Nano Lett.* **17**, 5027–5034 (2017).

137. Geim, A. K. & Grigorieva, I. V. Van der Waals heterostructures. *Nature* **499**, 419–425 (2013).

138. Li, D. *et al.* Multimodal Nonlinear Optical Imaging of MoS2 and MoS2-Based van der Waals Heterostructures. *ACS Nano* **10**, 3766–3775 (2016).

139. Chen, H. *et al.* Transition-metal dichalcogenides heterostructure saturable absorbers for ultrafast photonics. *Opt. Lett.* **42**, 4279–4282 (2017).

140. Brongersma, M. L. The road to atomically thin metasurface optics. *Nanophotonics* **10**, 643–654 (2021).

141. Popkova, A. A. *et al.* Nonlinear Exciton-Mie Coupling in Transition Metal Dichalcogenide Nanoresonators. *Laser Photonics Rev.* **16**, 2100604 (2022).

142. Panmai, M., Xiang, J., Zhou, L., Li, S. & Lan, S. Revealing Mie Resonances with Enhanced and Suppressed Second-Order Nonlinear Optical Responses in a Hexagonal-Prism-Like MoS2 Nanoparticle. *Laser Photonics Rev.* **17**, 2300346 (2023).

143. Zograf, G. *et al.* Combining ultrahigh index with exceptional nonlinearity in resonant transition metal dichalcogenide nanodisks. Preprint at https://doi.org/10.48550/arXiv.2308.11504 (2023).

144. Biswas, R., Prosad, A., Krishna, L. & Raghunathan, V. Enhanced four wave mixing from MoS2 disks supporting higher-order anapole resonance. in *2D Photonic Materials and Devices VI* vol. 12423 30–34 (SPIE, 2023).

145. Nauman, M. *et al.* Tunable unidirectional nonlinear emission from transition-metal-dichalcogenide metasurfaces. *Nat. Commun.* **12**, 5597 (2021).

146. Shi, J. *et al.* Giant Enhancement and Directional Second Harmonic Emission from Monolayer WS2 on Silicon Substrate via Fabry-Pérot Micro-Cavity. *ACS Nano* **16**, 13933–13941 (2022).

147. Du, J. *et al.* An on-Si directional second harmonic generation amplifier for MoS2/WS2 heterostructure. *Nano Res.* **16**, 4061–4066 (2023).

148. Kühner, L. *et al.* High-Q Nanophotonics over the Full Visible Spectrum Enabled by Hexagonal Boron Nitride Metasurfaces. *Adv. Mater.* **35**, 2209688 (2023).

149. Löchner, F. J. F. *et al.* Hybrid Dielectric Metasurfaces for Enhancing Second-Harmonic Generation in Chemical Vapor Deposition Grown MoS2 Monolayers. *ACS Photonics* **8**, 218–227 (2021).

150. Liu, Z. *et al.* Giant Enhancement of Continuous Wave Second Harmonic Generation from Few-Layer GaSe Coupled to High-Q Quasi Bound States in the Continuum. *Nano Lett.* **21**, 7405–7410 (2021).

151. Bernhardt, N. *et al.* Quasi-BIC Resonant Enhancement of Second-Harmonic Generation in WS2 Monolayers. *Nano Lett.* **20**, 5309–5314 (2020).

152. Mikheeva, E. *et al.* Space and Time Modulations of Light with Metasurfaces: Recent Progress and Future Prospects. *ACS Photonics* **9**, 1458–1482 (2022).

153. Hentschel, M. *et al.* Dielectric Mie voids: confining light in air. *Light Sci. Appl.* **12**, 3 (2023).

154. Liu, C.-H. *et al.* Developing ultrathin light emitters and metalenses based on Van der Waals materials. in *2D Photonic Materials and Devices II* vol. 10920 1092005 (SPIE, 2019).

155. Tonkaev, P., Sinev, I. S., Rybin, M. V., Makarov, S. V. & Kivshar, Y. Multifunctional and Transformative Metaphotonics with Emerging Materials. *Chem. Rev.* **122**, 15414–15449 (2022).

156. Qin, F. *et al.* π-phase modulated monolayer supercritical lens. *Nat. Commun.* **12**, 32 (2021).

157. Moon, S.-W., Kim, Y., Yoon, G. & Rho, J. Recent Progress on Ultrathin Metalenses for Flat Optics. *iScience* **23**, (2020).

158. Peng, Y. *et al.* Metalens in Improving Imaging Quality: Advancements, Challenges, and Prospects for Future Display. *Laser Photonics Rev.* **n/a**, 2300731.

159. Wang, X., Sun, Y. & Liu, K. Chemical and structural stability of 2D layered materials. *2D Mater.* **6**, 042001 (2019).

160. Gao, J. *et al.* Aging of Transition Metal Dichalcogenide Monolayers. *ACS Nano* **10**, 2628–2635 (2016).

161. Zhou, Q., Chen, Q., Tong, Y. & Wang, J. Light-Induced Ambient Degradation of Few-Layer Black Phosphorus: Mechanism and Protection. *Angew. Chem. Int. Ed.* **55**, 11437–11441 (2016).

162. Hu, Z. *et al.* Water-Catalyzed Oxidation of Few-Layer Black Phosphorous in a Dark Environment. *Angew. Chem. Int. Ed.* **56**, 9131–9135 (2017).

163. Huang, W. *et al.* Encapsulation strategies on 2D materials for field effect transistors and photodetectors. *Chin. Chem. Lett.* **33**, 2281–2290 (2022).

164. Long, G. *et al.* Type-controlled nanodevices based on encapsulated few-layer black phosphorus for quantum transport. *2D Mater.* **3**, 031001 (2016).

165. Chen, X. *et al.* High-quality sandwiched black phosphorus heterostructure and its quantum oscillations. *Nat. Commun.* **6**, 7315 (2015).

166. Wells, S. A. *et al.* Suppressing Ambient Degradation of Exfoliated InSe Nanosheet Devices via Seeded Atomic Layer Deposition Encapsulation. *Nano Lett.* **18**, 7876–7882 (2018).

167. Hu, X. *et al.* Halide-Induced Self-Limited Growth of Ultrathin Nonlayered Ge Flakes for High-Performance Phototransistors. *J. Am. Chem. Soc.* **140**, 12909–12914 (2018).

168. Jia, J. *et al.* Plasma-Treated Thickness-Controlled Two-Dimensional Black Phosphorus and Its Electronic Transport Properties. *ACS Nano* **9**, 8729–8736 (2015).

169. Wang, G. *et al.* Introduction of Interfacial Charges to Black Phosphorus for a Family of Planar Devices. *Nano Lett.* **16**, 6870–6878 (2016).

170. Huang, Y. L. *et al.* The organic–2D transition metal dichalcogenide heterointerface. *Chem. Soc. Rev.* **47**, 3241–3264 (2018).

171. Sun, J. *et al.* 2D–Organic Hybrid Heterostructures for Optoelectronic Applications. *Adv. Mater.* **31**, 1803831 (2019).

172. Kang, K. *et al.* High-mobility three-atom-thick semiconducting films with wafer-scale homogeneity. *Nature* **520**, 656–660 (2015).

173. Lee, Y.-H. *et al.* Synthesis of Large-Area MoS2 Atomic Layers with Chemical Vapor Deposition. *Adv. Mater.* **24**, 2320–2325 (2012).

174. Heiserer, S. *et al.* Controllable and Reproducible Growth of Transition Metal Dichalcogenides by Design of Experiments. *Adv. Electron. Mater.* **9**, 2300281 (2023).

175. Zhang, Y., Tan, Y.-W., Stormer, H. L. & Kim, P. Experimental observation of the quantum Hall effect and Berry's phase in graphene. *Nature* **438**, 201–204 (2005).

176. Novoselov, K. S. *et al.* Electric Field Effect in Atomically Thin Carbon Films. *Science* **306**, 666–669 (2004).

177. Geim, A. K. & Novoselov, K. S. The rise of graphene. *Nat. Mater.* **6**, 183–191 (2007).

178. Liu, S. *et al.* Nanopatterning Technologies of 2D Materials for Integrated Electronic and Optoelectronic Devices. *Adv. Mater.* **34**, 2200734 (2022).

179. Kollipara, P. S., Li, J. & Zheng, Y. Optical Patterning of Two-Dimensional Materials. *Research* **2020**, (2020).

180. Nicolosi, V., Chhowalla, M., Kanatzidis, M. G., Strano, M. S. & Coleman, J. N. Liquid Exfoliation of Layered Materials. *Science* **340**, 1226419 (2013).

181. Coleman, J. N. *et al.* Two-Dimensional Nanosheets Produced by Liquid Exfoliation of Layered Materials. *Science* **331**, 568–571 (2011).

182. Paton, K. R. *et al.* Scalable production of large quantities of defect-free few-layer graphene by shear exfoliation in liquids. *Nat. Mater.* **13**, 624–630 (2014).

183. Lin, Z. *et al.* Solution-processable 2D semiconductors for high-performance large-area electronics. *Nature* **562**, 254–258 (2018).

184. Li, J. *et al.* Printable two-dimensional superconducting monolayers. *Nat. Mater.* **20**, 181–187 (2021).

Biography:

Zeng Wang earned his doctorate from the School of Physical and Mathematical Sciences at Nanyang Technological University in Singapore. He now holds the position of Senior Scientist at the Institute of Materials Research and Engineering (IMRE), under the Agency for Science, Technology and Research (A*STAR). Wang's research focuses on metaoptics, two-dimensional optoelectronics, and advanced high-resolution optical lithography techniques.

K V Sreekanth is currently working as a Senior Scientist in the Institute of Materials Research and Engineering (IMRE), A*STAR, Singapore. He has received his PhD degree from Nanyang Technological University, Singapore. His research interests include nanophotonics, metasurfaces, phase change materials, and biosensors.

Meng Zhao received her PhD degree from National University of Singapore (NUS) in 2014. She is currently working as a Senior Scientist in the Institute of Materials Research and Engineering (IMRE), A*STAR, Singapore. Her current research interests focus mainly on the preparation and optoelectronics of novel 2D materials.

Jinpeng Nong received his PhD from the College of Optoelectronic Engineering, Chongqing University, China. He is currently a Senior Scientist in the Institute of Materials Research and Engineering (IMRE), A*STAR. His research interests include plasmonics and nanophotonics, 2D optoelectronics, mid-infrared spectroscopy and photodetection.

Yincheng Liu received his Bachelor of Arts degree from University of Oxford. He is currently a research engineer in the Institute of Materials Research and Engineering (IMRE), A*STAR. He is

currently working on characterization of optoelectronic devices made of two-dimensional materials.

Jinghua Teng received his PhD from the Department of Electrical and Computer Engineering, National University of Singapore. He is currently a Senior Principal Scientist and Senior Group Leader in the Institute of Materials Research and Engineering (IMRE), A*STAR. His research interests include nanophotonics, metamaterials and metasurfaces, 2D optoelectronics, and THz technology.